

SYNTHESIS AND ELECTROCHEMICAL CHARACTERIZATION OF 1,12-DIFERROCENYLDODECANE-TAGGED SELF-ASSEMBLED MONOLAYERS

By

Richard L. Porter

Richard L. Porter

I hereby release this thesis to the public and understand that this thesis will be made available from the OhioLink ETD Center and the Maag Library Circulation Desk for public access. I also authorize the University or other individuals to make copies of this thesis as needed for scholarly research.

Signature:

Submitted in Partial Fulfillment of the Requirements

for the Degree of

Richard L. Porter, Student

4/14/05
Date

Master of Science

Approvals:

In the

Larry S. Curtin, Ph.D., Advisor

Chemistry

4/15/05
Date

Program

Allen D. Hunter, Ph.D., Committee Member

4/15/05
Date

Timothy R. Wagner, Ph.D., Committee Member

4/15/05
Date

Youngstown State University

May, 2005

Peter J. Kasvinsky, Ph.D., Dean of Graduate Studies

4/14/05
Date

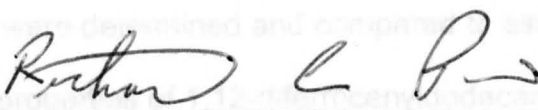
SYNTHESIS AND ELECTROCHEMICAL CHARACTERIZATION OF 1,12-DIFERROCENYLDODECANE-TAGGED SELF-ASSEMBLED MONOLAYERS

By

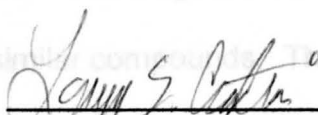
Richard L. Porter


I hereby release this thesis to the public. I understand that this thesis will be made available from the OhioLink ETD Center and the Maag Library Circulation Desk for public access. I also authorize the University or other individuals to make copies of this thesis as needed for scholarly research.

Signature:

 4/15/05
Richard L. Porter, Student Date

Approvals:

 4/15/05
Larry S. Curtin, Ph.D., Thesis Advisor Date

 4/15/05
Allen D. Hunter, Ph.D., Committee Member Date

 4/15/05
Timothy R. Wagner, Ph.D., Committee Member Date

 4/14/05
Peter J. Kasvinsky, Ph.D., Dean of Graduate Studies Date

ABSTRACT

The synthesis of 1,12-diferrocenyldodecane and subsequently 6-(diferrocenyldodecanylcarbonyl)pentanethiol was completed according to the protocol detailed here. The intermediate and final products were characterized by mass spectrometry, ^1H and ^{13}C NMR, as applicable. Two of the intermediate compounds; 1,12-diferrocenyldodecane-1,12-dione and 1,12-diferrocenyldodecane were analyzed via solution cyclic voltammetry. The formal potentials, ΔE_p values, chemical and electrochemical reversibility and diffusion control of the electron transfer process were determined and compared to established values. The electrochemical properties of 1,12-diferrocenyldodecane-tagged self-assembled monolayers adsorbed on gold electrodes were evaluated and compared to data obtained for similar compounds. The full width at half-maximum (FWHM), ΔE_p 's, formal potentials, degree of chemical and electrochemical reversibility, heterogeneous electron transfer rate constants, and surface coverages were determined for the inner and outer ferrocenes. A low ratio (8%) of surface coverage for the outer compared to the inner ferrocene was observed. The possible factors that may have led to the electrochemical inaccessibility of the outer ferrocene are discussed.

ACKNOWLEDGEMENTS

Mrs. Nellie J. Porter, Mother, 1925-2003

Mrs. Kathleen J. Porter, Wife

Miss Josie L. Porter, Daughter

Dr. Larry S. Curtin, Thesis Advisor

Dr. Allen D. Hunter, Committee Member

Dr. Tim R. Wagner, Committee Member

Mrs. Valerie Meyers

Mr. Jeff Meyers

Dr. Brian J. Saldanha, DuPont

Mr. Christopher Roe, DuPont

Youngstown State University

1.3 Monolayer Cyclic Voltammetry 8

1.4 Electrochemically Tagged Self-Assembled Monolayers 15

1.5 Research Proposal 19

1.6 References 20

Chapter 2 Experimental 21

2.1 Overview of Synthetic Procedure 21

2.2 Experimental 25

2.2.1 Chemicals 25

2.2.2 Instrumentation 25

2.2.3 Synthesis of 1,12-diferrocenyl dodecane-1,12-dione 26

Table of Contents

	Title Page	
	Signature Page	
	Abstract	iii
	Acknowledgements	iv
	Table of Contents	v
	List of Tables	viii
	List of Figures	ix
Chapter 1	Introduction	1
	1.1 Introduction to Self-Assembled Monolayers	1
	1.2 Solution Cyclic Voltammetry	5
	1.3 Monolayer Cyclic Voltammetry	8
	1.4 Diferrocene Tagged Self-Assembled Monolayers	15
	1.5 Research Proposal	19
	1.6 References	20
Chapter 2	Experimental	21
	2.1 Overview of Synthetic Procedure	21
	2.2 Experimental	25
Chapter 3	Electrochemistry	25
	2.2.1 Chemicals	25
	2.2.2 Instrumentation	25
	2.2.3 Synthesis of 1,12-diferrocenyldodecane-1,12-dione	26

2.2.4	¹ H NMR and mass spectrometry Data For 1,12-diferrocenyl dodecane-1,12-dione	27
2.2.5	Synthesis of 1,12-diferrocenyldodecane	27
2.2.6	¹ H NMR and mass spectrometry data for 1,12-diferrocenyldodecane	27
2.2.7	Synthesis of 6-(diferrocenyldodecanylcarbonyl)pentanebromide	28
2.2.8	¹ H NMR and mass spectrometry data for 6-(diferrocenyldodecanylcarbonyl)pentanebromide	28
2.2.9	Synthesis of 6-(diferrocenyldodecanylcarbonyl)pentanethiol	29
2.2.10	¹ H, ¹³ C NMR and mass spectrometry data for 6-(diferrocenyldodecanylcarbonyl)pentanethiol	29
2.3	Results and Discussion	30
2.3.1	Characterization of 1,12-diferrocenyldodecane-1,12-dione	30
2.3.2	Characterization of 1,12-diferrocenyldodecane	32
2.3.2	Characterization of 6-(diferrocenyldodecanyl carbonyl)pentanebromide	38
2.3.3	Characterization of 6-(diferrocenyldodecanyl carbonyl)pentanethiol	41
2.4	Conclusions	51
2.5	References	53
Chapter 3	Electrochemistry	54
3.1	Introduction	54
3.2	Chemicals	54
3.3	Instrumentation	55

3.4	Experimental	55
3.4.1	Electrode Preparation	55
3.4.2	Solution Voltammetry	56
3.4.3	Monolayer Voltammetry	56
3.5	Results / Discussion	57
3.5.1	Solution Voltammetry	57
3.5.2	Monolayer Voltammetry	63
3.5.3	Conclusions	76
3.5.4	References	80

List of Tables

Table 3.1	Surface coverages of 6-(diferrocenyldodecanyl carbonyl)pentanethiol monolayers on gold electrodes	72
Figure 1.1		4
Figure 1.2	Cyclic voltammetry experiment	6
Figure 1.3	Cyclic voltammogram of a mixed ferrocene monolayer	10
Figure 1.4	Cyclic voltammogram illustrating scan rate dependence of a ferrocene monolayer	12
Figure 1.5	Biferrocene terminated alkanethiols on gold	18
Figure 2.1	Synthetic procedure	19
Figure 2.2	¹ H NMR spectrum of 1,12-diferrocenyldodecane-1,12-dione	21
Figure 2.3	Mass spectrum of 1,12-diferrocenyldodecane-1,12-dione	33
Figure 2.4	Fragments from mass spectrum of 1,12-diferrocenyldodecane-1,12-dione	34
Figure 2.5	¹ H NMR spectrum of 1,12-diferrocenyldodecane	35
Figure 2.6	Mass spectrum of 1,12-diferrocenyldodecane	36
Figure 2.7	Fragments from mass spectrum of 1,12-diferrocenyldodecane	37
Figure 2.8	¹ H NMR spectrum of 6-(diferrocenyldodecanyl carbonyl)pentanebromide, aliphatic region	38
Figure 2.9	¹ H NMR spectrum of 6-(diferrocenyldodecanyl carbonyl)pentanebromide, ferrocene region	40
Figure 2.10	Mass spectrum of 6-(diferrocenyldodecanyl carbonyl)pentanebromide	42
Figure 2.11	Fragments from mass spectrum of 6-(diferrocenyldodecanyl carbonyl)pentanebromide	43

List of Figures

Figure 1.1	Ferrocene monolayer on a gold electrode	4
Figure 1.2	Cyclic voltammetry experiment	6
Figure 1.3	Cyclic voltammogram of a mixed ferrocene monolayer	10
Figure 1.4	Cyclic voltammogram illustrating scan rate dependence of a ferrocene monolayer	12
Figure 1.5	Biferrocene terminated alkanethiols on gold	16
Figure 2.1	Synthetic procedure	22
Figure 2.2	^1H NMR spectrum of 1,12-diferrocenyldodecane-1,12-dione	31
Figure 2.3	Mass spectrum of 1,12-diferrocenyldodecane-,12-dione	33
Figure 2.4	Fragments from mass spectrum of 1,12-diferrocenyldodecane-1,12-dione	34
Figure 2.5	^1H NMR spectrum of 1,12-diferrocenyldodecane	35
Figure 2.6	Mass spectrum of 1,12-diferrocenyldodecane	36
Figure 2.7	Fragments from mass spectrum of 1,12-diferrocenyldodecane	37
Figure 2.8	^1H NMR spectrum of 6-(diferrocenyldodecanyl carbonyl)pentanebromide, aliphatic region	39
Figure 2.9	^1H NMR spectrum of 6-(diferrocenyldodecanyl carbonyl)pentanebromide, ferrocene region	40
Figure 2.10	Mass spectrum of 6-(diferrocenyldodecanyl carbonyl)pentanebromide	42
Figure 2.11	Fragments from mass spectrum of 6-(diferrocenyldodecanylcarbonyl)pentanebromide	43

Figure 2.12	¹ H NMR spectrum of 6-(diferrocenyldodecanyl carbonyl)pentanethiol, aliphatic region	44
Figure 2.13	¹ H NMR spectrum of 6-(diferrocenyldodecanyl carbonyl)pentanethiol, ferrocene region	46
Figure 2.14	¹³ C NMR spectrum of 6-(diferrocenyldodecanyl carbonyl)pentanethiol, aliphatic region	48
Figure 2.15	¹³ C NMR spectrum of 6-(diferrocenyldodecanyl carbonyl)pentanethiol, ferrocene region	50
Figure 2.16	MALDI mass spectrum of 6-(diferrocenyldodecanyl carbonyl)pentanethiol	52
Figure 3.1	Cyclic voltammogram of 0.1 mM 1,12-diferrocenyl dodecane-1,12-dione in 0.1 M TBAP / CH ₃ CN	58
Figure 3.2	Plot of anodic peak currents vs. the square root of scan rate for 1,12-diferrocenyldodecane-1,12-dione	60
Figure 3.3	Cyclic voltammogram of 0.1 mM 1,12-diferrocenyl dodecane in 0.1 M TBAP / CH ₃ CN	61
Figure 3.4	Plot of anodic peak currents vs. the square root of scan rate for 1,12-diferrocenyldodecane	62
Figure 3.5	Cyclic voltammogram of a 6-(diferrocenyl dodecanylcarbonyl)pentanethiol monolayer on electrode E11 in 1 M HClO ₄	64
Figure 3.6	Cyclic voltammogram of a 6-(diferrocenyl dodecanylcarbonyl)pentanethiol monolayer on electrode E12 in 1 M HClO ₄	65
Figure 3.7	Effect of increasing scan rate from 100 to 400 mV/sec on peak broadening of voltammetric waves for a 6-(diferrocenyldodecanylcarbonyl)pentanethiol monolayer on electrode E11	67
Figure 3.8	Plot of anodic peak currents vs. scan rate for a 6-(diferrocenyldodecanylcarbonyl)pentanethiol monolayer on electrode E11	70

Figure 3.9	Plot of anodic peak currents vs. scan rate for a 6-(diferrocenyldodecanylcarbonyl)pentanethiol monolayer on electrode E12	71
Figure 3.10	Effect of increasing bridging alkane chain length in diferrocene-tagged alkanethiol SAM's on electrochemical accessibility of outer ferrocene	79

1.1 Introduction

Self-assembled monolayers have been studied extensively due to their use in providing an empirical basis for the construction of interfacial devices such as sensors and transducers that utilize directional electron transfer.¹ Self-assembly techniques work well for molecules that bond strongly to a surface and have shapes that pack well in two dimensions.² Furthermore, self-assembly chemistry offers significant advantages over other approaches to electrode modification.

Two common types of organic monolayers are Langmuir-Blodgett (L-B) films and organosilanes. Though the technique is technically not self-assembly, Langmuir-Blodgett films are formed by immersing a hydrophilic substrate in a solution containing amphiphilic molecules. Mechanical compression of the substrate as it is removed from solution yields a film with the hydrophilic end at the surface and the hydrophobic end of the molecule away from the surface.^{3,4} The disadvantages of the films include, a surface film which is not reproducible due to many defect sites, a non-ordered surface and intrinsic instability.^{1,2,5} Furthermore, forming Langmuir-Blodgett films often requires cleanroom facilities.

Organosilane monolayers are formed by reacting an organosilane (i.e. trialkoxyalkylsilane) with a hydroxylated surface, such as platinum or silica, yielding a strong covalent bond between monolayer and substrate.⁶ The primary

CHAPTER ONE

INTRODUCTION

1.1 Introduction to Self-Assembled Monolayers

Self-assembled monolayers have been studied extensively due to their use in providing an empirical basis for the construction of interfacial devices such as sensors and transducers that utilize directional electron transfer.¹ Self-assembly techniques work well for molecules that bond strongly to a surface and have shapes that pack well in two dimensions.² Furthermore, self-assembly chemistry offers significant advantages over other approaches to electrode modification.

Two common types of organic monolayers are Langmuir-Blodgett (L-B) films and organosilanes. Though the technique is technically not self-assembly, Langmuir-Blodgett films are formed by immersing a hydrophilic substrate in a solution containing amphiphilic molecules. Mechanical compression of the substrate as it is removed from solution yields a film with the hydrophilic end at the surface and the hydrophobic end of the molecule away from the surface.^{3,4} The disadvantages of the films include; a surface film which is not reproducible due to many defect sites, a non-ordered surface and intrinsic instability.^{1,2,5} Furthermore, forming Langmuir-Blodgett films often requires cleanroom facilities.

Organosilane monolayers are formed by reacting an organosilane (i.e. with triethoxyalkylsilane) with a hydroxylated surface, such as platinum or silica, yielding a strong covalent bond between monolayer and substrate.⁴ The primary

advantage of silane films is that because they are covalently bonded to the surface, they are much more robust than Langmuir-Blodgett films. The disadvantages include; disorder, a large head group, water sensitivity, considerable tertiary structure and less close packing than seen in Langmuir-Blodgett or alkanethiol films.^{1,2,4-6} Self-assembled monolayers have also been formed from disulfides, sulfides and fatty acids on metal oxides.⁵ Here, we consider self-assembled monolayers that consist of unsubstituted and ferrocene terminated *n*-alkanethiols on gold electrodes.⁵

The advantages of using *n*-alkanethiols for making self-assembled monolayers are that they are commercially available, stable and relatively easy to prepare.¹⁻⁶ The degree of ordering can be controlled and the monolayers can be highly ordered.¹⁻⁶ Furthermore, alkanethiol SAM's are not sensitive to water and do not require a clean room for manufacture. Alkanethiol SAM's are synthesized by simply immersing the appropriate substrate (Au, Cu, Ag, Hg) in a stirred solution of the thiol overnight.¹⁻⁷ The bond that is formed between the thiol and the gold electrode is very strong, with an energy of 30-40 kcal/mole.⁴ Due to lateral van der Waals forces, the alkane chains are held in an all *trans* configuration and exhibit more order with increasing chain length.³

Order is affected by the size of the head group, chain length, size of the terminal group and the nature of substrate.¹⁻⁵ The sulfur headgroup is similar in size to the alkane chain, contributing to increased order.⁸ For alkane chains with less than 6 carbons, the monolayers tend to be disordered, 6-12 are more liquid like, and with more than 12 carbons the monolayers tend to be crystalline,

exhibiting a high degree of order.⁶ The longer the alkane chain length, the more order the monolayers exhibit since the lateral van der Waals forces between the chains increases.³ Large or bulky terminal groups may cause the monolayer to be less crystalline and have a higher degree of disorder.⁸ Substrates that are not smooth can have many defect sites and significantly decrease the degree of order in the monolayer. Mixed monolayers of ferrocene-terminated thiols that are diluted with *n*-alkanethiols can exhibit the behavior of a well ordered structure.⁷ However, at high mole fractions of the electroactive thiol, the amount of disorder in a monolayer will increase, possibly because of interactions between ferrocene sites and inhomogeneity in the film.⁵

After synthesis, ferrocene alkanethiols are typically characterized by mass spectrometry, proton and ¹³C NMR and UV-Vis spectroscopy.⁵ A structural representation of a monolayer formed by co-adsorption of ferrocene-terminated alkanethiols and unsubstituted alkanethiols on gold is presented in Figure 1.1.⁵

Cyclic voltammetry can be used to characterize ferrocene substituted and unsubstituted alkanethiol self-assembled monolayers. Self-assembled monolayers are an ideal system for determining sequencing in interfacial electron transfer.⁵ Since ferrocene is an electroactive molecule that has been extremely well characterized and is a neutral, reversible, outer-sphere redox-active molecule, it is an ideal choice for incorporation into self-assembled monolayers.² Moreover, self-assembled monolayers containing ferrocene enable redox processes within a well defined chemical environment.² Other redox active

monolayers studied include ruthenium pentammines, porphyrins, and anthraquinones.^{1,2,3} Here the focus is on electroactive ferrocene groups (Ferrocene, $\text{Fc} = (\eta^5\text{-C}_5\text{H}_5)_2\text{Fe}$) which are typically connected to a gold electrode via an alkanethiol chain.⁴

1.2 Solution Voltammetry

Solution voltammograms are often characterized by cyclic voltammetry, a technique where the potential of the working electrode is scanned from an initial value (E_i) to a pre-determined switching potential (E_s). At the switching potential, the voltage is scanned back to the initial potential (E_i) at the same scan rate. As shown in Figure 1.2,⁵ voltammograms are plotted as current (i) versus potential (E). The voltammogram shown in Figure 1.2, the potential of the electrode is first scanned in the cathodic direction causing the tendency of electrons in the metal to increase. Initially, currents are associated with the migration in response to the change in electrode potential. Once a potential negative enough to reduce the analyte is reached, electrons are transferred from the metal to the analyte.

Figure 1.1: Representation of a self-assembled monolayer formed by co-adsorption of ferrocene-terminated and unsubstituted alkanethiols on gold.⁵

reaches a peak and then tails off because the surface concentration of the analyte is driven to zero, causing concentration polarization. Concentration polarization occurs when electron transfer kinetics are slow with respect to diffusion. Thus, the current drops off from the peak value due to mass transport limitations. At the switching potential, the scan is reversed and the reduced form

monolayers studied include ruthenium pentammines, porphyrins, and anthroquinones.^{1,3,8} Here the focus is on electroactive ferrocene groups (Ferrocene, $\text{Fc}=(\eta^5\text{-C}_5\text{H}_5)\text{Fe}(\eta^5\text{-C}_5\text{H}_5)$) which are typically connected to a gold electrode via an *n*-alkanethiol chain.³

1.2 Solution Cyclic Voltammetry

Ferrocene compounds in solution are often characterized by cyclic voltammetry, a potentiodynamic technique where the potential of the working electrode is scanned from an initial value (E_i) to a pre-determined switching potential (E_λ).⁸ At the switching potential, the voltage is scanned back to the initial potential (E_i) at the same scan rate. As shown in Figure 1.2.⁹

Voltammograms are plotted as current (y-axis) versus potential (x-axis). In the voltammogram shown in Figure 1.2, the potential of the electrode is first scanned in the cathodic direction, causing the energy of electrons in the metal to increase. Initially, currents are non-faradaic and are a function of ion migration in response to the change in electrode potential. Once a potential negative enough to reduce the analyte is reached, electrons are transferred from the metal to the analyte, resulting in an increase in current due to reduction of the analyte.³ Currents associated with electron transfer are called faradaic currents. The current reaches a peak and then tails off because the surface concentration of the analyte is driven to zero, causing concentration polarization. Concentration polarization occurs when electron transfer kinetics are rapid with respect to diffusion. Thus, the current drops off from the peak value due to mass transport limitations. At the switching potential, the scan is reversed and the reduced form

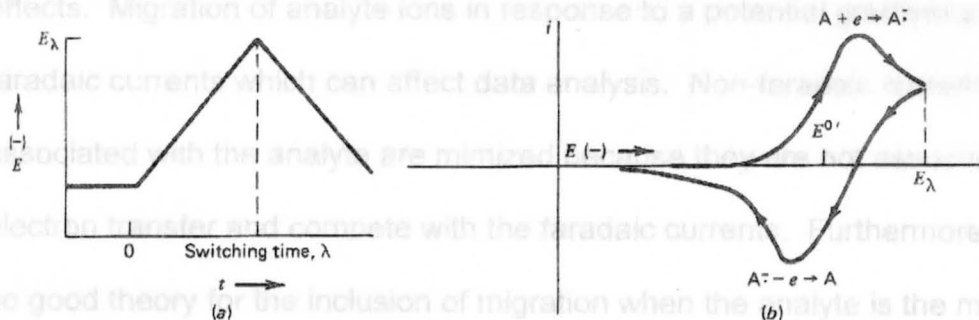
of the analyte generated in the cathodic scan is re-oxidized, producing an anodic current, which again falls off due to concentration polarization.^{8,9} Redox potentials ($E^{0'}$ s) or formal potentials are determined as the average of the anodic and cathodic peak potentials.⁸

Solution voltammetry experiments differ from monolayer voltammetry experiments in their sensitivity to mass transport. Mass transport consists of diffusion, migration and hydrodynamic effects. In cyclic voltammetry experiments, the solutions are typically not stirred, eliminating hydrodynamic effects.

Migration of analyte ions in response to a potential sweep can affect data analysis. Non-faradaic currents associated with the analyte are minimized by the use of a supporting electrolyte. Electron transfer and compete with the faradaic current. Furthermore, there is no good theory for the inclusion of migration when the analyte is the migrating species.⁸ To minimize analyte migration, a large excess of non-electroactive supporting electrolyte is used, so that electrolyte ions are present to migrate in response to the changing electrode potential.⁸ Statistically, there are many more electrolyte ions available, so migration of the analyte is minimized and mass transport of the analyte depends solely on diffusion.⁸ Diffusion control in solution voltammetry is observed when the peak currents are proportional to the square root of the scan rate.⁹

Figure 1.2: Description of a cyclic voltammetry experiment.⁹

Cyclic voltammetry can be used to determine the chemical reversibility of a redox reaction. A chemically irreversible reaction is one in which a chemical change occurs before or after the electron transfer i.e. dimerisation or dimer



of the analyte generated in the cathodic scan is re-oxidized, producing an anodic current, which again tails off due to concentration polarization.^{8,9} Redox potentials (E° 's) or formal potentials are determined as the average of the anodic and cathodic peak potentials.⁹

Solution voltammetry experiments differ from monolayer voltammetry experiments in their sensitivity to mass transport. Mass transport consists of diffusion, migration and hydrodynamic effects. In cyclic voltammetry experiments, the solutions are typically not stirred, eliminating hydrodynamic effects. Migration of analyte ions in response to a potential gradient are non-faradaic currents which can affect data analysis. Non-faradaic currents associated with the analyte are minimized because they are not associated with electron transfer and compete with the faradaic currents. Furthermore, there is no good theory for the inclusion of migration when the analyte is the migrating species.³ To minimize analyte migration, a large excess of non-electroactive supporting electrolyte is used, so that electrolyte ions are present to migrate in response to the changing electrode potential.³ Statistically, there are many more electrolyte ions available, so migration of the analyte is minimized and mass transport of the analyte depends solely on diffusion.³ Diffusion control in solution voltammetry is observed when the peak currents are proportional to the square root of the scan rate.⁹

Cyclic voltammetry can be used to determine the chemical reversibility of a redox reaction. A chemically irreversible reaction is one in which a chemical change occurs before or after the electron transfer i.e. decomposition or dimer

formation.⁹ Chemical reversibility refers to the relative stability of the reactants and products, and whether all of the species that are reduced in the forward scan are re-oxidized in the reverse scan. For a chemically reversible process, the ratio of the peak anodic to peak cathodic currents is equal to 1. Peak current ratios not equal to 1 indicate a chemically irreversible reaction.⁹

Electrochemical reversibility is determined by whether or not the Nernst equation is obeyed at all applied potentials.⁹ The absence of an increase in peak splitting with increasing scan rate indicates that the rate of electron transfer is rapid on the voltammetric time scale. If the charge transfer kinetics are slow, the anodic and cathodic peaks in the voltammogram move apart with increasing scan rate. For slow electron transfers, a heterogeneous electron transfer rate constant can be calculated via the method of Laviron.¹¹

1.3 Monolayer Cyclic Voltammetry

In a ferrocene containing monolayer cyclic voltammetry experiment an increasing anodic potential is applied and the current response is measured in the same fashion as discussed with solution voltammetry. However, in monolayer voltammetry the analyte is confined to the surface of the gold electrode, therefore diffusional mass transport is not a concern.³ Furthermore, the presence of a surface confined species is indicated by the peak currents being proportional to scan rate instead of the square root of the scan rate.^{1,2,5} The amount of electroactive ferrocene in the monolayer can be quantified from cyclic voltammograms by integration of the faradaic currents.⁵ The ratio of anodic to cathodic peak currents can be used in the same fashion as solution

voltammetry to ascertain chemical reversibility. ΔE_p values of approximately 0 mV that are independent of scan rate indicate electrochemical reversibility.⁵ Electrochemical irreversibility is indicated by increasing values of ΔE_p with increasing scan rate.

Electron transfer kinetics can be measured as a function of potential and temperature, and can also be studied as a function of alkanethiol chain length.^{5,6,7} Li and Weaver¹² determined that electron transfer kinetics between an electrode and electroactive groups attached to the surface through carbon chains drops off exponentially with increasing chain length. Finklea & Hanshaw⁷ reported that varying the length of the polymethylene chains allowed the distance dependence of the rate of electron transfer to be directly probed. They reported that the primary determinant of the standard rate constant is chain length.⁷

At slow scan rates (1-100 mV/sec), cyclic voltammograms reveal that the cathodic and anodic current peaks occur at similar or the same potentials for a surface confined ferrocene.¹ Figure 1.3¹ illustrates the scan rate dependence of a mixed alkanethiol monolayer containing both ferrocene terminated and unsubstituted thiols. At higher scan rates the anodic and cathodic current peaks split apart, indicating that the voltammetric time scale is comparable to the rate of electron transfer.¹ Peak splittings can be converted to a standard heterogeneous electron transfer rate constant using a method described by Laviron.¹³ For an electrochemically irreversible process, Laviron's method shows that as ΔE_p increases at a given scan rate, the heterogeneous electron transfer rate decreases.^{3,13} Based on a graph of $n\Delta E_p$ vs $1/m$, where;

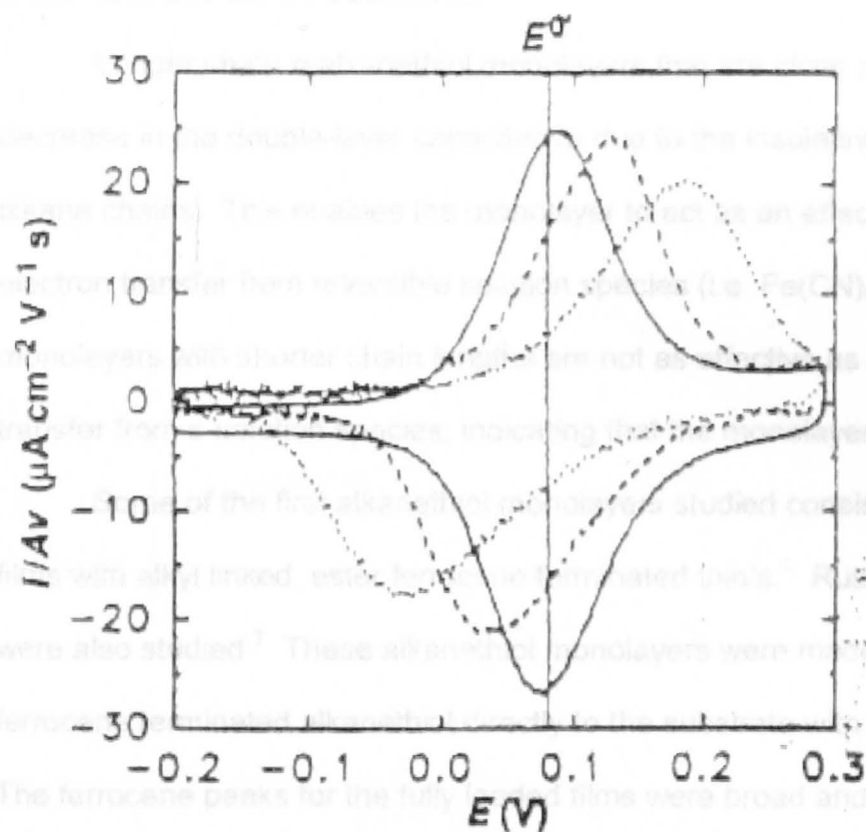


Figure 1.3: Cyclic voltammograms of a mixed monolayer of 0.1 mM ferrocene terminated alkanethiol and 0.9 mM unsubstituted alkanethiols on gold illustrating the scan rate dependence of ΔE_p .¹ (10 mV/sec=solid line, 120 mV/sec=dashed, 500 mV/sec=dotted)

$$1/m = (nFv) / (RTk^{\circ})$$

a rate constant can be determined.¹¹

Longer chain *n*-alkanethiol monolayers that are close packed exhibit a decrease in the double-layer capacitance due to the insulating nature of the alkane chains. This enables the monolayer to act as an effective barrier to electron transfer from reversible solution species (i.e. $\text{Fe}(\text{CN})_6^{3-/4-}$).³ However, monolayers with shorter chain lengths are not as effective as barriers to electron transfer from a solution species, indicating that the monolayers are disordered.

Some of the first alkanethiol monolayers studied consisted of fully loaded films with alkyl linked, ester ferrocene terminated thiols.⁵ Ruthenium pentamines were also studied.⁷ These alkanethiol monolayers were made by attaching the ferrocene terminated alkanethiol directly to the substrate with a polar ester group. The ferrocene peaks for the fully loaded films were broad and asymmetric, as shown in Figure 1.4.⁵ The non-ideal behavior, in the form of peak broadening and reversible electron transfer is attributable to a large number of defect sites in the monolayer.^{3,5} Monolayers with low mole fractions of alkanethiols attached to ferrocene via a polar ester group show ideal electrochemistry and indicate that the ferrocene groups are homogenous and non-interacting.⁵ This is because at low surface coverages, the ferrocenes occupy nearly identical electroactive sites.

Mixed monolayers are formed by co-adsorbing electroactive thiols and diluent alkanethiols having no electroactive ferrocene group.⁵ In most mixed monolayers, the chain length of the substituted and unsubstituted thiols are usually similar. Typically, the mole fraction of ferrocene in the coating solution is

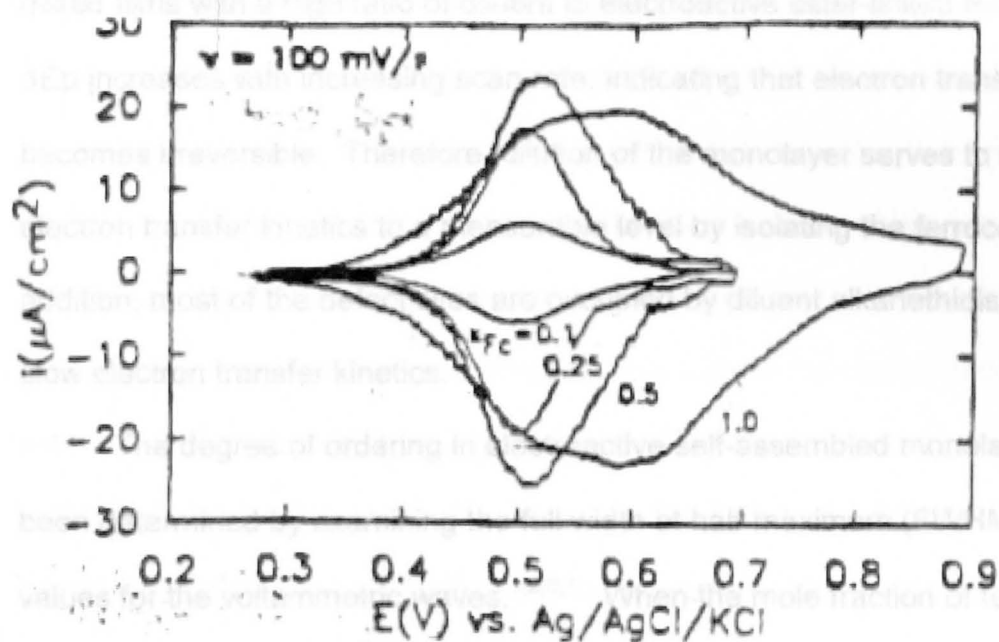


Figure 1.4: A cyclic voltammogram in 1M HClO_4 of mixed monolayers of $(\text{FcCO}_2(\text{CH}_2)_{11}\text{SH})$ and $\text{CH}_3(\text{CH}_2)_9\text{SH}$ formed from ethanol solutions containing various mole fractions of the ferrocene-terminated thiol.⁵ (@ a scan rate of 100 mV/sec)

nearly the same as the mole fraction adsorbed in the monolayer. Chidsey¹ found that dilution led to better-defined and narrower peaks in the voltammetry. Typically, the ratio of peak currents for both fully loaded and mixed ferrocene containing monolayers is one indicating chemical reversibility. However, for mixed films with a high ratio of diluent to electroactive ester-linked ferrocenes, ΔE_p increases with increasing scan rate, indicating that electron transfer becomes irreversible. Therefore, dilution of the monolayer serves to slow the electron transfer kinetics to a measurable level by isolating the ferrocenes.⁵ In addition, most of the defect sites are occupied by diluent alkanethiols, resulting in slow electron transfer kinetics.

The degree of ordering in electroactive self-assembled monolayers has been determined by examining the full width at half-maximum (FWHM) or k° values for the voltammetric waves.^{1,2,5,7} When the mole fraction of ferrocene is less than or equal to 0.25, ferrocene oxidation and reduction peaks are symmetrical with FWHM's of approximately $90/n$ mV, indicating that the monolayer is ordered.⁵ Furthermore, a heterogenous electron transfer rate constant, k° , can be measured. At higher mole fractions of ferrocene, the voltammetric waves broaden considerably, indicating that there is an increase in disorder in the films.¹⁰ A cyclic voltammogram plotted as current density versus potential for mixed monolayers containing various fractions of ferrocene-terminated and unsubstituted thiols were presented in Figure 1.4.⁵ The absence of peak splitting indicates that the rate of electron transfer is rapid at high ferrocene mole fractions.^{2,5} Finklea & Hanshaw⁵ and Chidsey¹ reported that as

the coverage of ferrocene increases, cyclic voltammograms tend to become broad and ill defined, since there are more defect sites and subsequently the electroactive ferrocenes are not in the same environment. If the ferrocenes are not in the same environment, then they have slightly different formal potentials (E° 's), which leads to broader waves. In addition, electron transfer rates become too rapid to be measured due to fast electron hopping in the disordered films.

It has been reported that increasing the alkyl chain length in mixed monolayers containing both ferrocene terminated and unsubstituted thiols does not drastically affect the ferrocene surface coverage.⁵ However, as the chain length of the unsubstituted thiol increases (for a given ferrocene terminated alkanethiol chain length) the surface coverages of the ferrocene terminated thiols in the monolayers decrease.⁵ This is due to the lower solubility of the alkanethiols in the ethanol coating solutions, and their higher affinity for adsorption.⁵ Rowe and Creager² determined that for ferrocenes with alkanethiols shorter than six carbons, ferrocene adsorption is favored and for alkanethiols greater than six carbons in length, alkanethiol adsorption is favored.

As alkanethiol co-adsorbate chain length increases above that of the ferrocene alkane chain length, there is a corresponding shift in redox potential to more positive values.² Both peaks shift together, indicating that this is a thermodynamic effect.⁷ Essentially, at longer diluent chain lengths, upon oxidation the charge compensating anion is being forced to reside in a non-polar environment. This results in a larger overpotential for ferrocene oxidation.

The occurrence of an intermolecular reaction for Bfc^{2+}

A shift in redox potentials in environments that incur ion-pairing effects was discovered by Rowe and Creager.² They determined that ion pairing was occurring between oxidized ferricinium and perchlorate². They concluded that as the environment surrounding the ferrocenes becomes more alkane-like with increasing alkanethiol co-adsorbate length, ion pairing of ferricinium becomes more favorable, resulting in larger ion-pairing constants.² This more 'alkane-like' environment, leads to a positive shift in the redox potential for ferrocene oxidation and increased ion-pairing effects between ferricinium and ClO_4^- .²

1.4 Diferrocene Tagged Self-Assembled Monolayers

With all of the recent work conducted on ferrocene terminated and unsubstituted alkanethiol self-assembled monolayers, only a handful of researchers have examined diferrocene terminated alkanethiol self-assembled monolayers.^{3,8,10,14,15} Horikoshi et al.¹⁴ have synthesized self-assembled monolayers of $\text{Bfc-CO(CH}_2)_7\text{SH}$ ($\text{Bfc}=1,1'$ -biferrocenyl). A schematic of the substitution method of preparing octanethiol-stabilized gold clusters is presented in Figure 1.5.¹⁴ Kubo et al.¹⁵ reported different decomposition kinetics between Bfc^+ and Bfc^{2+} and a strong dependence of the electron transfer rate constant on the concentration of biferrocenyl units in the self-assembled monolayer.

Decomposition of Bfc^+ is a second order (i.e. intermolecular) reaction since a plot of the inverse of surface coverage vs. the number of scans shows a linear relationship.¹⁵ However, the decomposition of Bfc^{2+} is first order, because the log of the surface coverage increases (or is linear) with increasing scan rate (as opposed to scan rate $^{1/2}$).¹⁵ The occurrence of an intramolecular reaction for Bfc^{2+}

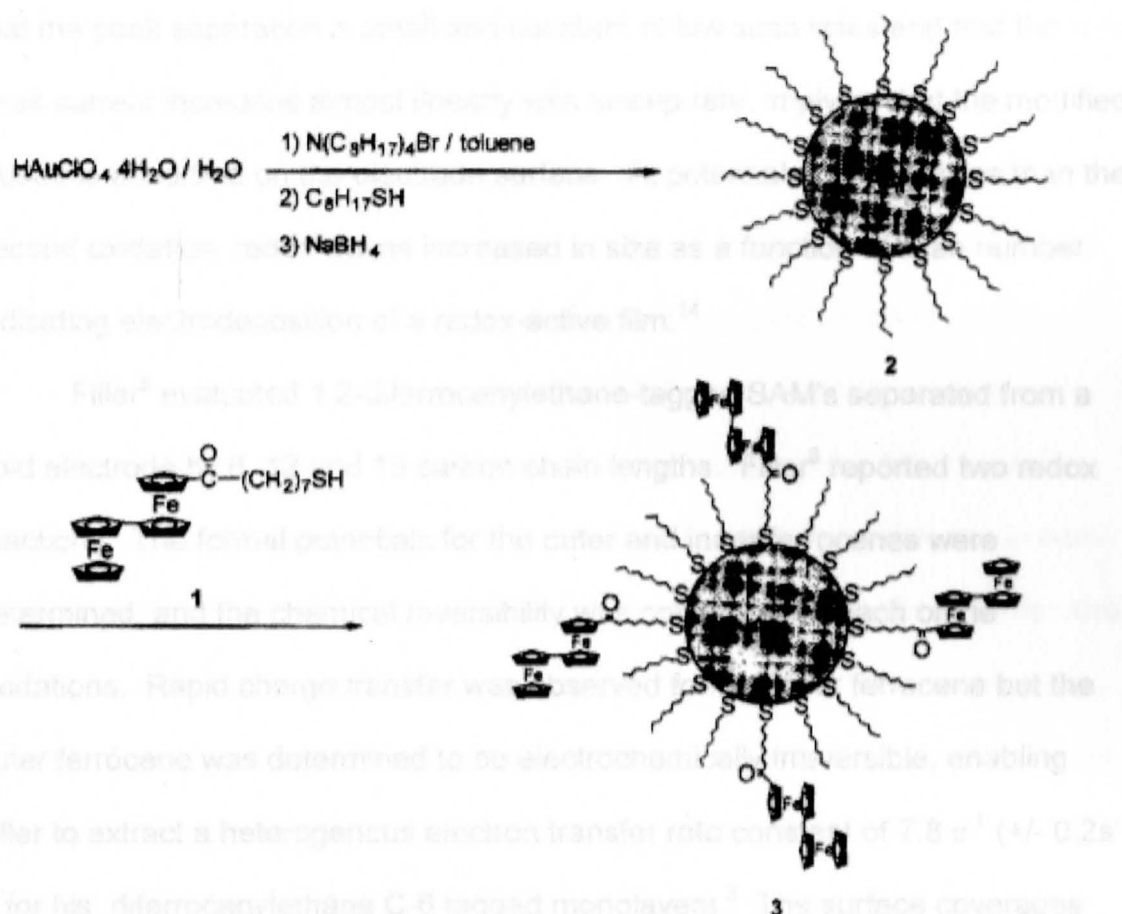


Figure 1.5: Preparation of gold clusters modified with biferrrocenyl-terminated alkanethiols prepared by the substitution method of octanethiol-stabilized gold clusters.¹⁴

was deduced by Kubo.¹⁵ Horikoshi et al.'s¹⁴ experiments also have indicated that the peak separation is small and constant at low scan rates and that the peak current increases almost linearly with sweep rate, implying that the modified cluster is adsorbed on the electrode surface. At potentials more positive than the second oxidation, redox waves increased in size as a function of scan number, indicating electrodeposition of a redox-active film.¹⁴

Filler⁸ evaluated 1,2-diferrocenylethane-tagged SAM's separated from a gold electrode by 6, 12 and 16 carbon chain lengths. Filler⁸ reported two redox reactions. The formal potentials for the outer and inner ferrocenes were determined, and the chemical reversibility was confirmed for each of the oxidations. Rapid charge transfer was observed for the inner ferrocene but the outer ferrocene was determined to be electrochemically irreversible, enabling Filler to extract a heterogeneous electron transfer rate constant of 7.8 s^{-1} ($\pm 0.2 \text{ s}^{-1}$) for his diferrocenylethane C-6 tagged monolayers.⁸ The surface coverages were similar for both ferrocenes in the monolayer, and the dependence of peak currents on scan rate indicated a surface confined species. The FWHM values of the voltammetric waves were examined, with values typically larger than $90/n$ mV, indicating the monolayers were somewhat disordered. However, the degree of order was found to decrease with increasing alkane chain length.

Pugh³, studied 6-(diferrocenylohexanecarbonyl)pentanethiol SAM's to determine the effects of a longer chain length between the ferrocenes. The purpose of this was to determine to what extent an electron hopping mechanism occurs.³ The monolayers Pugh³ studied were also characterized by two redox

reactions. The voltammetric data was evaluated and the electron transfer was determined to be chemically reversible for both waves. The oxidation of the inner ferrocenes was electrochemically reversible, but oxidation of the outer ferrocenes was found to be electrochemically irreversible and a rate constant of 11.9 s^{-1} ($\pm 0.2 \text{ s}^{-1}$) was determined.³ The monolayer was found to be surface confined. Of interest, the surface coverage of the outer ferrocenes were only 40% of that of the inner ferrocenes. Pugh³ suggested that this may be due to the outer ferrocenes folding over into the non-polar bridging region of the film. Lewis¹⁶ further studied 6-(difluorenylhexanoyl)pentanethiol monolayers, in non-aqueous solvents (0.1 M TBAP in THF) to determine if the outer ferrocenes were folding over into the non-polar hexane region of the film, thus becoming electrochemically inaccessible.¹⁶ Lewis¹⁶ also reported that the outer ferrocenes were less accessible than the inner ferrocenes. It was determined that desorption had occurred in the 0.1M TBAP in THF solutions and an increase in the surface coverage of the outer ferrocenes was not noted.¹⁶ In other words, the ratio of surface coverages (outer/inner) was the same for both 1M HClO₄ and 0.1M TBAP in THF electrolytes.¹⁶ This indicated that the use of non-aqueous 0.1M TBAP in THF did not increase the electrochemical accessibility of the outer ferrocenes. Finally, Pugh³ observed FWHM values indicating a good degree of order in all of the waves except for the first anodic wave. This wave showed a FWHM value of $44.9/n \text{ mV}$, which was not typical of a surface confined species.³ A structural rearrangement or domain formation upon oxidation of the outer ferrocenes was suggested as one reason that this might be occurring.³

1.5 Research Proposal

This research will focus on the synthesis, characterization and electrochemical properties of diferrocene substituted alkanethiol monolayers. 1, 12-diferrocenyldodecane will be synthesized, characterized and tagged with an alkanethiol chain. It will then be adsorbed onto gold electrodes for electrochemical evaluation. Sub-problems include: 1.) Synthesis and characterization of the diferrocenyldodecane-tagged *n*-alkanethiol. 2.) Synthesis and electrochemical characterization of diferrocenyldodecane-terminated self-assembled monolayers on gold electrodes. 3.) Determination of the electrochemical properties of the monolayers. This will include a possible shift in formal potentials (E° 's), chemical and electrochemical reversibility, presence of a surface confined species, the relative surface coverages of the inner and outer ferrocenes, full-width at half maximum peak height for the voltammetric waves, and the rates of electron transfer. All of the parameters discussed will be compared to those obtained by Filler⁸ and Pugh.³ To date, the synthesis, characterization and electron transfer kinetics of self-assembled alkanethiol monolayers tagged with diferrocenyldodecane have not yet been determined.

14. Honkoshi, T.; Itoh, M.; Kurihara, M.; Kubo, K.; Nishihara, H. *J. Electroanal. Chem.*, 1999, 473, 113-116.

15. Kubo, K.; Kondow, H.; Nishihara, H. *Electrochemistry* 1999, 67, (12), 1129-1131.

16. Lewis, W. L. An Electrochemical Study of the Kinetic and Thermodynamic Properties of 8-(Diferrocenyloctyl)carboxylic Acid Self-Assembled Monolayers, M.S. Thesis, Youngstown State University, August 2002.

1.6 References

1. Chidsey, C. E. D. *Science* **1991**, *251*, 919-921.
2. Rowe, G. K.; Creager, S. E. *Langmuir* **1991**, *7*, 2307-2312.
3. Pugh, C. A. Synthesis and Electrochemical Characterization of Novel Bridged Ferrocene Tagged Alkanethiol Self-Assembled Monolayers, M.S. Thesis, Youngstown State University, May 2001.
4. Ulman, A. *An Introduction to Ultrathin Organic Films*; Academic Press: New York, **1994**.
5. Chidsey, C. E. D. ; Bertozzi, C. R.; Putvinski, T. M., Majsce, A. M. *J. Am. Chem. Soc.* **1990**, *112*, 4301-4306.
6. Finklea, H.O.; Ravenscroft, M.S.; Snider, D.A. *Langmuir* **1993**, *9*, 223-227.
7. Finklea, H.O.; Hanshew, D.D. *J. Am. Chem. Soc.*, **1992**, *114*, 3173.
8. Filler, W. J. Characterization of Diferrocene Tagged Self-Assembled Alkanethiol Monolayers, M.S. Thesis, Temple University, August, 1996.
9. Bard, A., Faulkner, L. *Electrochemical Methods*, 2nd ed. Wiley: New York, **2000**.
10. Curtin, L.S.; Unpublished Results.
11. Laviron, E. J. *Electroanal. Chem* **1979**, *100*, 263-270.
12. Li, T. T.-T.; Weaver. M. *J. Am. Chem. Soc.* **1984**, *106*, 6107-6108
13. Laviron, E. J. *Electroanal. Chem* **1979**, *101*, 19-28.
14. Horikoshi, T.; Itoh, M.; Kurihara, M.; Kubo, K.; Nishihara, H J. *Electroanal. Chem.*, **1999**, *473*, 113-116.
15. Kubo, K.; Kondow, H.; Nishihara, H. *Electrochemistry* **1999**, *67*, (12), 1129-1131.
16. Lewis, W. L. An Electrochemical Study of the Kinetic and Thermodynamic Properties of 6-(Diferrocenylhexanylethyl)pentanethiol Self-Assembled Monolayers, M.S. Thesis, Youngstown State University, August 2002.

CHAPTER TWO

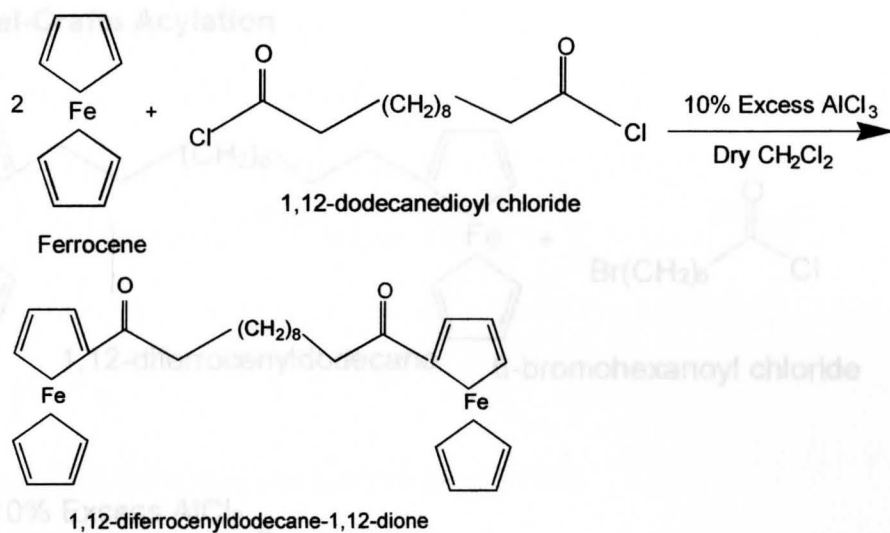
EXPERIMENTAL

2.1 Overview of Synthetic Procedure

The reaction sequence for the synthetic procedure is presented in Figure 2.1. The purpose of the synthesis was to make a ferrocene dimer bridged by 12 carbons. A 6 carbon alkanethiol chain was attached to one of the cyclopentadiene rings on the dimer for adsorption of the molecule onto a gold electrode. This was done in order to study the thermodynamics and electron transfer kinetics of the surface confined molecule. To date, a 12 carbon bridged ferrocene dimer has not been synthesized and characterized.¹⁻⁵

In a classic Friedel-Crafts acylation, ferrocene and 1,12-dodecanedioyl chloride were dissolved in dry, distilled methylene chloride. Aluminum chloride was then added as the Lewis acid to produce 1,12-diferrocenyldodecane-1,12-dione. In a Clemmensen reduction, 1,12-diferrocenyldodecane-1,12-dione was dissolved in toluene and combined with zinc dust dissolved in de-ionized water, mercuric chloride, and HCl were also added to reduce the carbonyls and yield fully reduced 1,12-diferrocenyldodecane. This product was reacted with 6-bromohexanoyl chloride in a Friedel-Crafts acylation under the above conditions to yield 6-(diferrocenyldodecanecarbonyl)pentanebromide. Finally, in the thiolation step, this compound was dissolved in ethanol and reacted with a large excess of sodium hydrosulfide to synthesize the desired product 6-(diferrocenyldodecanecarbonyl)pentanethiol.

Friedel-Crafts Acylation



Clemmensen Reduction

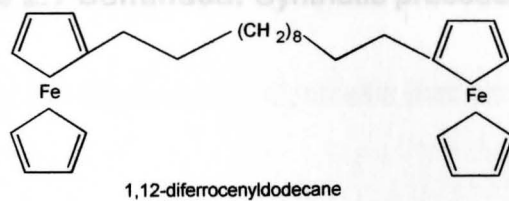
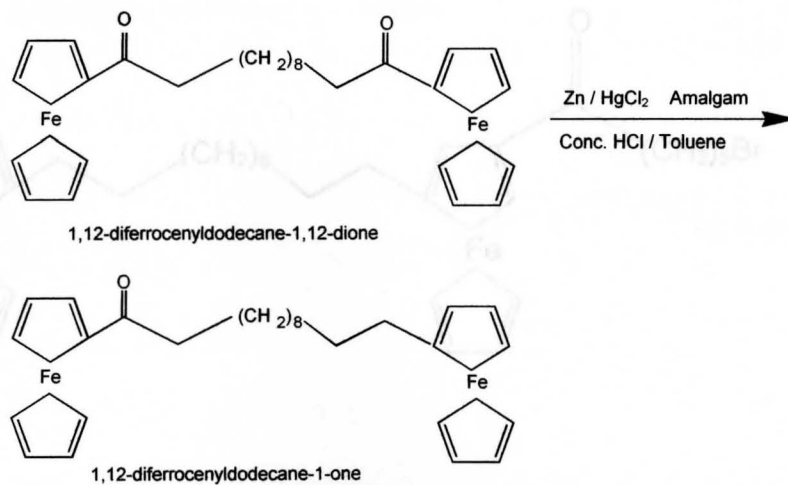


Figure 2.1: Synthetic procedure

Thiolation

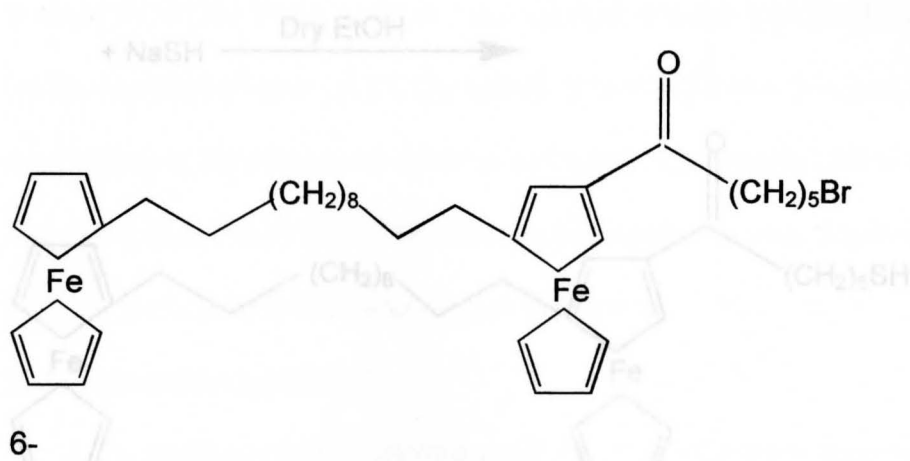
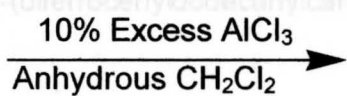
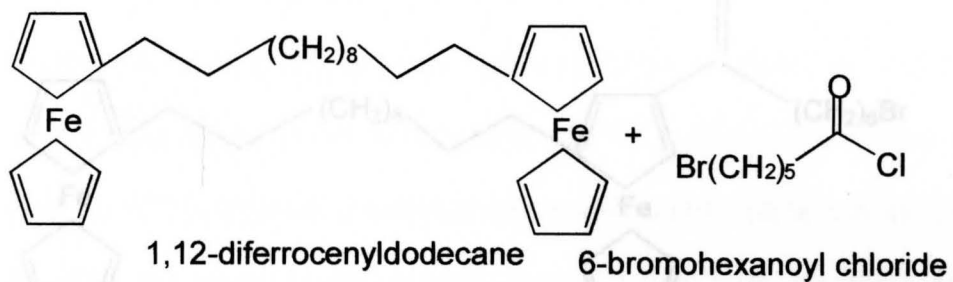
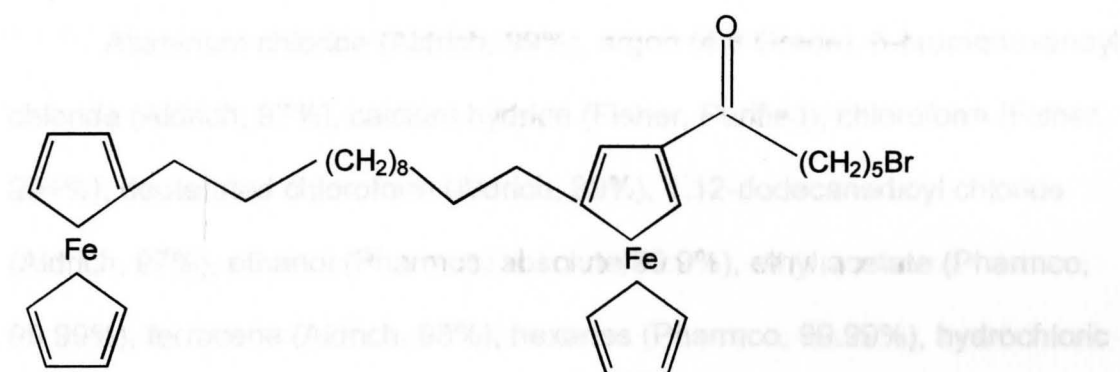
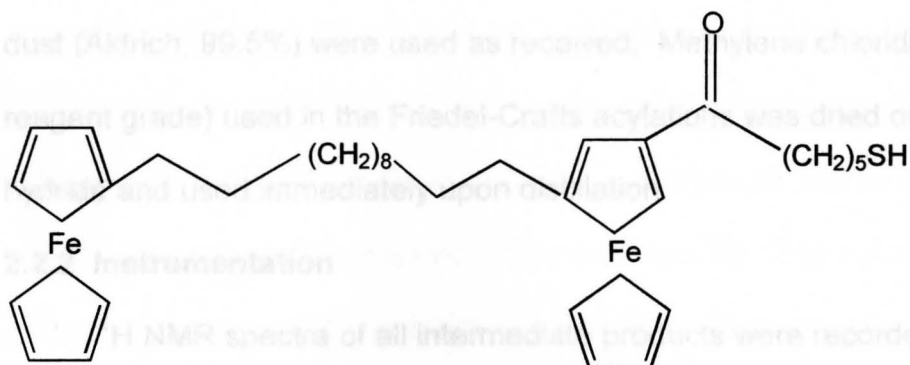
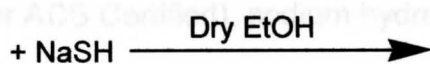
Friedel-Crafts Acylation**Figure 2.1 Continued: Synthetic procedure**

Figure 2.1 Continued: Synthetic procedure

Thiolation



6-(diferrocenyldodecanylcarbonyl)pentanebromide



6-(diferrocenyldodecanylcarbonyl)pentanethiol

Figure 2.1 Continued: Synthetic procedure

2.2 Experimental

2.2.1 Chemicals

Aluminum chloride (Aldrich, 99%), argon (4.8 Grade), 6-bromohexanoyl chloride (Aldrich, 97%), calcium hydride (Fisher, Purified), chloroform (Fisher, 99+%), deuterated chloroform (Aldrich, 99%), 1,12-dodecanedioyl chloride (Aldrich, 97%), ethanol (Pharmco, absolute 99.9%), ethyl acetate (Pharmco, 99.99%), ferrocene (Aldrich, 98%), hexanes (Pharmco, 99.99%), hydrochloric acid (Fisher, reagent grade), mercuric chloride (Aldrich, 98%), perchloric acid (Fisher, reagent grade), silica (Aldrich, 60Å, 200-400 mesh), sodium chloride (Fisher ACS Certified), sodium hydrosulfide (Fisher, hydrated), anhydrous sodium sulfate (Fisher, ACS Certified), toluene (Fisher, reagent grade), and zinc dust (Aldrich, 99.5%) were used as received. Methylene chloride (Fisher, reagent grade) used in the Friedel-Crafts acylations was dried over calcium hydride and used immediately upon distillation.

2.2.2 Instrumentation

^1H NMR spectra of all intermediate products were recorded with a Varian Gemini-2000 400 MHz spectrometer with reference to the deuterium signal of the solvent employed. ^1H and ^{13}C NMR of the final product were collected on a Varian Unity Inova 500 MHz spectrometer. Chemical shifts are reported in ppm downfield from tetramethylsilane. A Finnigan GCQ mass spectrometer was used to determine the parent ion and fragmentation pattern of some products. Fragmentation for the pentanebromide was collected on a Bruker Esquire LC-MS. The MALDI mass spectrum of the thiol was collected on a PerSeptives Biosystems Voyager-DE STR mass spectrometer.

2.2.3 Synthesis of 1,12-diferrocenyldodecane-1,12-dione

1,12-diferrocenyldodecane-1,12-dione was synthesized by a Friedel-Crafts acylation via a modified version of the method of Chidsey.² All glassware was dried overnight in an oven at 110 °C, and an overhead mechanical stirrer and a 1000 ml three neck flask were used during the reaction. Ferrocene (34.78 g, 0.187 mol) was dissolved in 250 ml of distilled methylene chloride that was cooled to 0 °C in an ice bath. 1,12-dodecanedioyl chloride (25g, 0.0935 mol) was added and the solution was stirred under static argon for approximately five minutes. Anhydrous aluminum chloride (27.42 g, 0.206 mol) was added and the solution immediately turned purple. The solution was allowed to warm to room temperature and stirring was continued for 1½ hours. Three hundred milliliters of de-ionized water was added drop-wise from an addition funnel and stirring was continued for an additional 1½ hours. The resulting reaction mixture was washed five times with de-ionized water until the aqueous layer was colorless. The mixture was dried with brine and anhydrous Na₂SO₄. The solvent was then removed under reduced pressure. The crude product was purified by column chromatography using silica as the stationary phase and 80% hexanes: 20% ethyl acetate as the mobile phase. The second band to come off the column ($R_f = 0.7-0.8$) contained the desired product, 1,12-diferrocenyldodecane-1,12-dione (5.4% yield). This synthetic procedure was repeated again with ferrocene (35.00 g, 0.188 mol), 1,12-dodecanedioyl chloride (25g, 0.0935 mol) and anhydrous aluminum chloride (27.50 g, 0.207 mol), to obtain more 1,12-diferrocenyldodecane-1,12-dione (12.2% yield).

2.2.4 ^1H NMR and MS Data for 1,12-diferrocenyldodecane-1,12-dione

^1H NMR (CDCl_3 , 400MHz, ppm) 1.322 (broad m, 12H, peak F), 1.701 (broad m, 4H, peak E), 2.692 (broad t, 4H, peak D), 4.194 (s, 10H, peak A), 4.487 (t, 4H, peak B), 4.780 (t, 4H, peak C).

Mass spectrometry: parent ion peak at 566 m/z.

2.2.5 Synthesis of 1,12-diferrocenyldodecane

A Clemmensen reduction was used to synthesize 1,12-diferrocenyldodecane.^{4,6} 1,12-diferrocenyldodecane-1,12-dione (9.02 g, 0.0158 mol) was dissolved in 850 ml of toluene and was mixed with a freshly prepared zinc / mercury amalgam; mercuric chloride (1.06 g, 0.039 mol) and zinc dust (15.79 g, 0.240 mol), 30 ml of de-ionized water and 40 ml of 12.1 M HCl. The biphasic solution was agitated with an overhead mechanical stirrer and refluxed under static argon for 20 hours. Two 30 ml portions of 12.1 M HCl were added with an addition funnel after 6 and 12 hours, respectively. Upon cooling, the organic phase was washed 3 times with de-ionized water and then 3 times with brine and dried over twenty grams of anhydrous Na_2SO_4 overnight. The crude product was purified by column chromatography using silica as the stationary phase and chloroform as the eluent. The first band ($R_f = 0.9$) contained the desired product, 1,12-diferrocenyldodecane (58.5% yield).

2.2.6 ^1H NMR and MS Data for 1,12-diferrocenyldodecane

^1H NMR (CDCl_3 , 400MHz, ppm) 1.199 (broad m, 16H, peak F), 1.417 (broad m, 4H, peak E), 2.228 (t, 4H, peak D), 3.976 (broad s, 4H, peak C), 3.996 (broad s, 4H, peak B), 4.032 (broad s, 10H, peak A).

Mass spectrometry: parent ion peak at 538 m/z.

2.2.7 Synthesis of 6-(diferrocenyldodecanylcarbonyl)pentanebromide

In a Friedel-Crafts acylation, 1,12-diferrocenyldodecane (5 g, 0.0093 mol) was placed in a three neck flask and dissolved in 100 ml of freshly distilled methylene chloride that had been cooled to 0 °C in an ice bath.^{2,7} 6-bromo hexanoyl chloride (2.73 g, 0.0128 mol) was added and the resultant mixture was stirred under static argon for approximately five minutes. Anhydrous aluminum chloride (1.36 g, 0.0102 mol) was then added and the solution turned dark purple. The solution was allowed to warm to room temperature and stirring was continued under static argon for 1½ hours. Fifty milliliters of distilled water was added dropwise through an addition funnel and the solution was stirred for an additional 1½ hours. The reaction mixture was washed 3 times with de-ionized water, 3 times with brine, and then was dried over anhydrous Na₂SO₄ overnight. The solvent was removed under reduced pressure and the crude product was separated by column chromatography using silica as the stationary phase and 85% hexanes: 15% ethyl acetate as the mobile phase. Band 2 (R_f = 0.7) contained the desired product (7.5% yield).

2.2.8 ¹H NMR and MS Data for 6-(diferrocenyldodecanylcarbonyl)pentane bromide

¹H NMR (CDCl₃, 400MHz, ppm) 1.224 ppm (broad s, 16H, peak F), 1.401 ppm (broad m, 2H, peak O), 1.493 ppm (broad m, 4H, peak E, G), 1.682 ppm (broad m, 2H, peak N), 1.890 ppm (t, 2H, peak P), 2.194 ppm (t, 2H, peak D), 2.321 ppm (d, 2H, peak H), 2.673 ppm (m, 2H, peak M), 3.407 ppm (t, 2H, peak Q), 4.027 ppm (broad m, 2H, peak C), 4.039 ppm (d, 2H, peak B), 4.089 ppm (s,

10H, peaks A,L), 4.376 ppm (m, 1H, peak I), 4.396 ppm (s, 1H, peak J), 4.660 ppm (t, 1H, peak K)

Mass spectrometry: parent ion peak occurs at 716 m/z.

2.2.9 Synthesis of 6-(diferrocenyldodecanylcarbonyl)pentanethiol

6-(diferrocenyldodecanylcarbonyl)pentanebromide (0.1274 g, 0.1779 mol) was dissolved in 70 ml of absolute ethanol that had been de-aerated for 2 hours by bubbling with argon through a Pasteur pipette. The ethanol was then added to the reaction flask and stirred under static argon. Hydrated sodium hydrosulfide (0.200 g, 3.568 mol) was dissolved in 50 ml of de-aerated ethanol and added slowly to the reaction mixture over an hour. The reaction was then stirred overnight. The reaction mixture was extracted three times with anhydrous ethyl ether and the organic layer was washed three times with brine. The ether was then removed under reduced pressure. The desired product, 6-(diferrocenyldodecanylcarbonyl)pentanethiol (band 3, $R_f = 0.4$) was purified via column chromatography using silica as the stationary phase and 95% hexanes : 5% ethyl acetate as the eluent (14% yield).

2.2.10 ^1H , ^{13}C NMR and MS Data for 6-(diferrocenyldodecanylcarbonyl)pentanethiol

^1H NMR (CDCl_3 , 400MHz, ppm) 1.207 ppm (s, 1H, peak R), 1.277 ppm (broad s, 18H, peak F,O), 1.439 ppm (broad m, 2H, peak G), 1.455 ppm (broad m, 2H, peak E), 1.470 ppm (broad m, 2H, peak P), 1.741 ppm (q, 2H, peak N), 2.230 ppm (t, 2H, peak H), 2.304 ppm (t, 2H, peak D), 2.351 ppm (broad m, 2H, peak Q), 2.709 ppm (broad m, 2H, peak M), 4.015 ppm (s, 2H, peak C), 4.049

ppm (s, 2H, peak B), 4.065 (s, 5H, peak A), 4.077 (s, 5H, peak L), 4.120 ppm (s, 1H, peak J), 4.422 (broad m, 1H, peak I), 4.670 (broad m, 1H, peak K).

^{13}C NMR (CDCl_3 , 500MHz, ppm) 23.197 ppm (peak G), 27.569 ppm (peak S), 28.374 ppm (peak R), 28.698 ppm (peaks F,H), 28.785 ppm (peak E), 28.909 ppm (peak I), 30.115 ppm (peak T), 30.348 ppm (peak U), 38.657 ppm (peak Q), 66.186 ppm (peak D), 67.279 ppm (peak C), 67.668 ppm (peak B), 68.160 ppm (peak A), 68.204 ppm (peak O), 68.831 ppm (peak J), 68.871 ppm (peak N), 69.446 ppm (peak K), 71.526 ppm (peak M), 72.000 ppm (peak L).

Mass spectrometry: Parent ion peak occurs at 667 m/z.

2.3 Results and Discussion

2.3.1 Characterization of 1,12-diferrocenyldodecane-1,12-dione

The ^1H NMR (Figure 2.2) shows the methylene protons (carbons 4 to 9) in the center of the alkane chain at 1.322 ppm (peak F). The protons on the number 3 and 10 carbons of the alkane chain appear at 1.701 ppm (peak E). The protons (carbons 2 and 11) immediately adjacent to the carbonyl are downfield at 2.692 ppm (peak D). The downfield shift of the protons (peaks D and E) is due to the carbonyl being an electron-withdrawing group. The peak at 4.194 ppm (peak A) represents the protons on the bottom cyclopentadienyl (Cp^-) rings. The peak at 4.487 ppm (peak B) is indicative of the protons three carbons from the carbonyl and the peak at 4.780 ppm (peak C) represents the protons two carbons away from the carbonyl.

Figure 2.2: ^1H NMR spectrum of 1,12-diferrocenyldodecane-1,12-dione

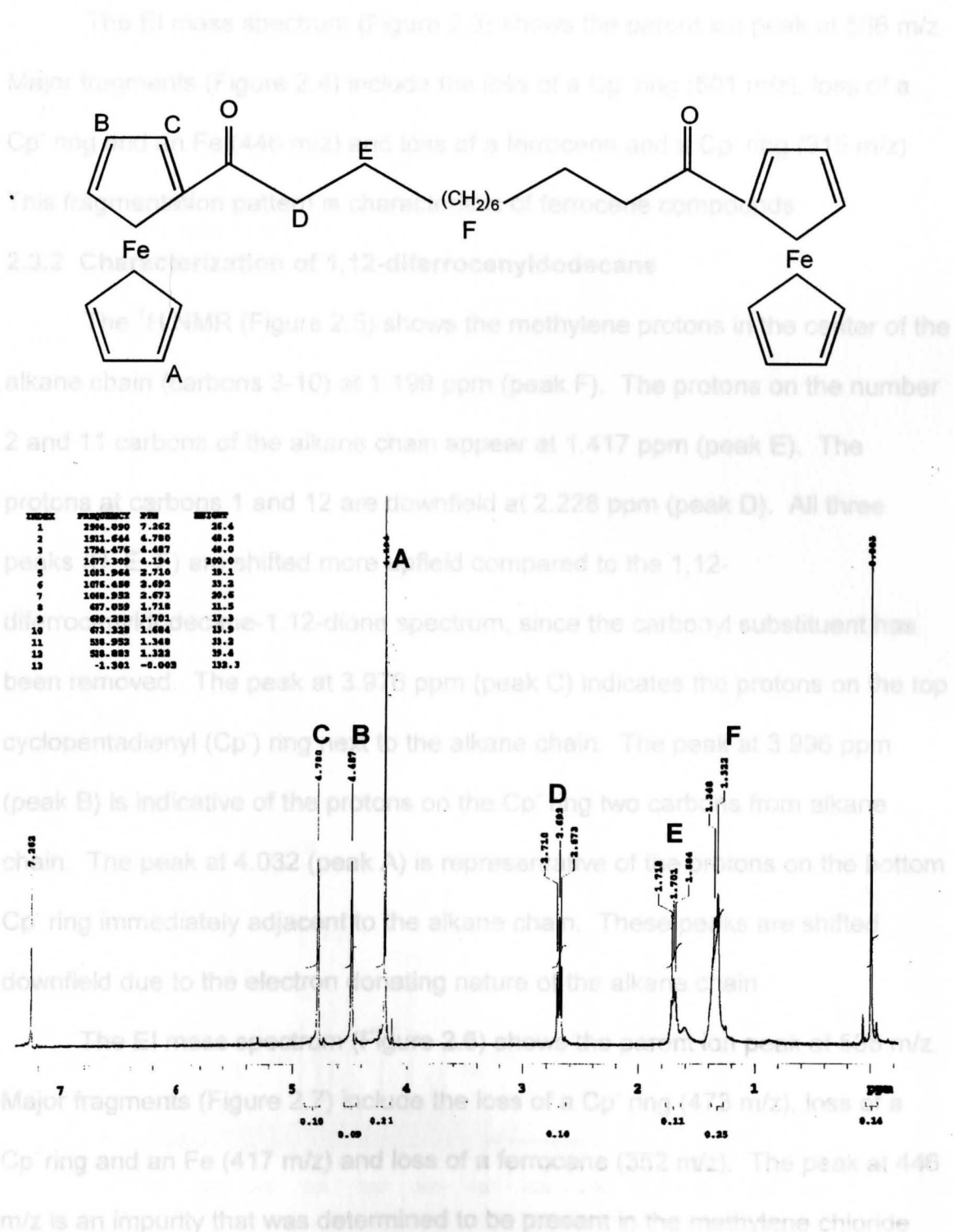


Figure 2.2: ^1H NMR spectrum of 1,12-diferrocenyldodecane-1,12-dione

The EI mass spectrum (Figure 2.3) shows the parent ion peak at 566 m/z. Major fragments (Figure 2.4) include the loss of a Cp⁻ ring (501 m/z), loss of a Cp⁻ ring and an Fe (446 m/z) and loss of a ferrocene and a Cp⁻ ring (315 m/z). This fragmentation pattern is characteristic of ferrocene compounds.

2.3.2 Characterization of 1,12-diferrocenyldodecane

The ¹H NMR (Figure 2.5) shows the methylene protons in the center of the alkane chain (carbons 3-10) at 1.199 ppm (peak F). The protons on the number 2 and 11 carbons of the alkane chain appear at 1.417 ppm (peak E). The protons at carbons 1 and 12 are downfield at 2.228 ppm (peak D). All three peaks (D, E, F) are shifted more upfield compared to the 1,12-diferrocenyldodecane-1,12-dione spectrum, since the carbonyl substituent has been removed. The peak at 3.976 ppm (peak C) indicates the protons on the top cyclopentadienyl (Cp⁻) ring next to the alkane chain. The peak at 3.996 ppm (peak B) is indicative of the protons on the Cp⁻ ring two carbons from alkane chain. The peak at 4.032 (peak A) is representative of the protons on the bottom Cp⁻ ring immediately adjacent to the alkane chain. These peaks are shifted downfield due to the electron donating nature of the alkane chain.

The EI mass spectrum (Figure 2.6) shows the parent ion peak at 538 m/z. Major fragments (Figure 2.7) include the loss of a Cp⁻ ring (473 m/z), loss of a Cp⁻ ring and an Fe (417 m/z) and loss of a ferrocene (352 m/z). The peak at 446 m/z is an impurity that was determined to be present in the methylene chloride solvent.

Figure 2.3: Mass spectrum of 1,12-diferrocenyldodecane-1,12-dione

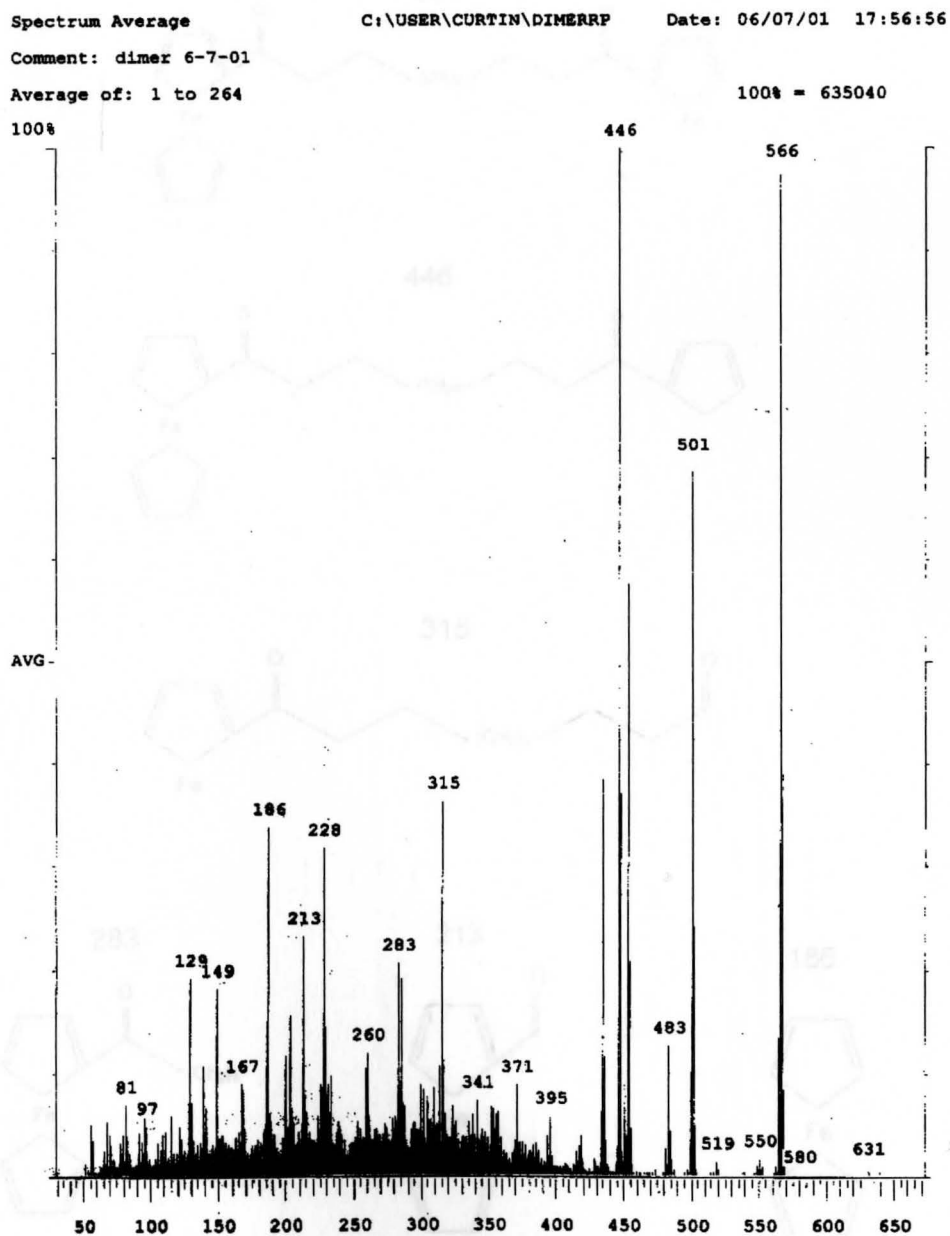


Figure 2.3: Mass spectrum of 1,12-diferrocenyldodecane-1,12-dione

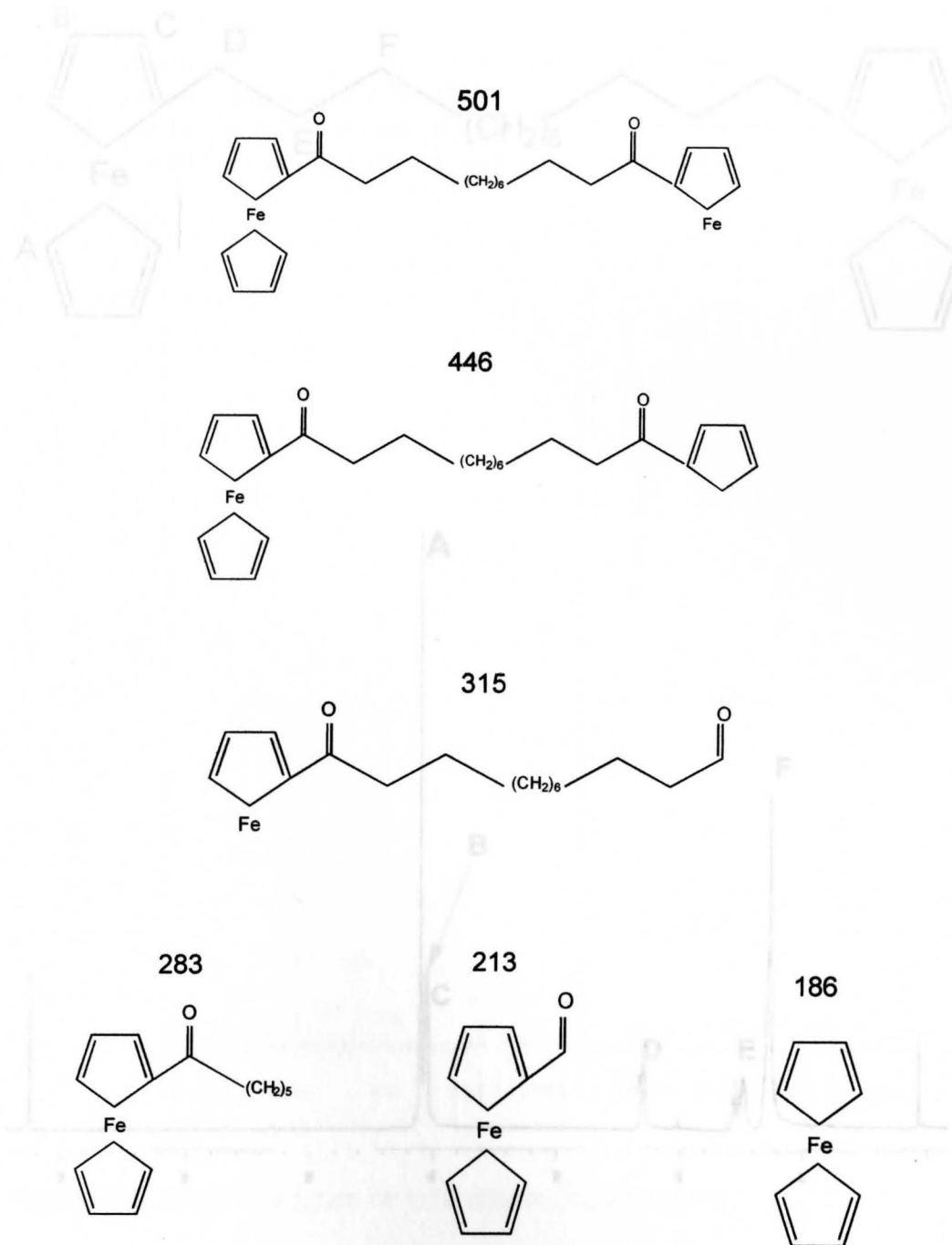


Figure 2.4: Major fragments (m/z) of 1,12-diferrocenyldodecane 1,12-dione mass spectrum

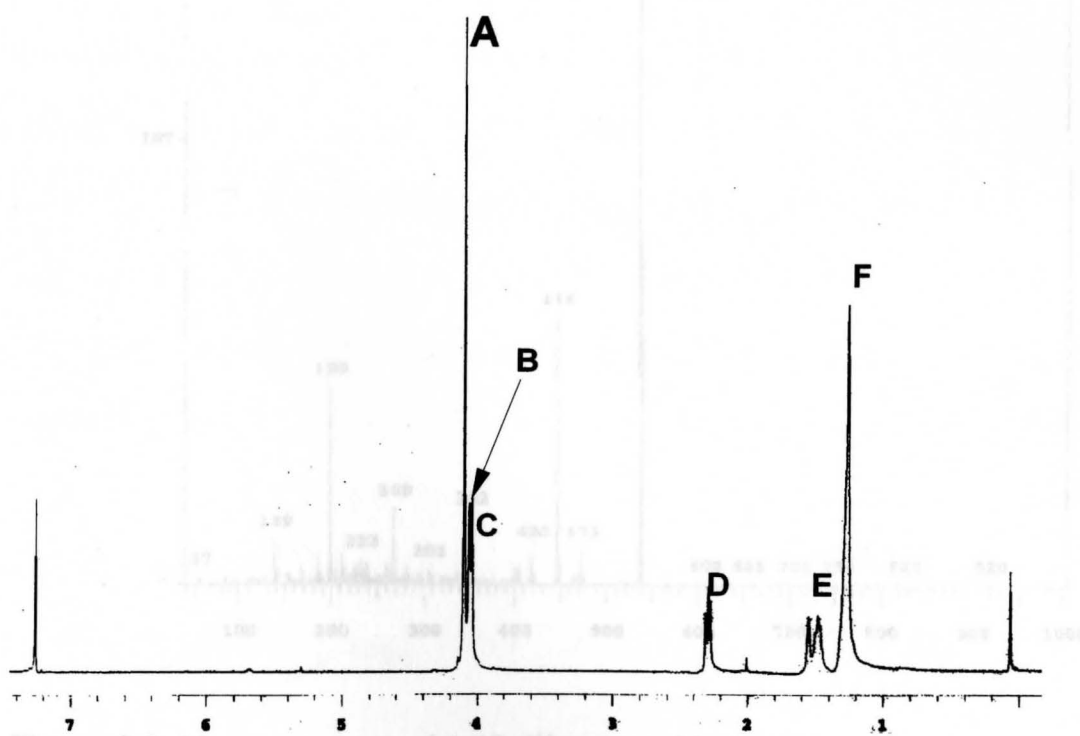
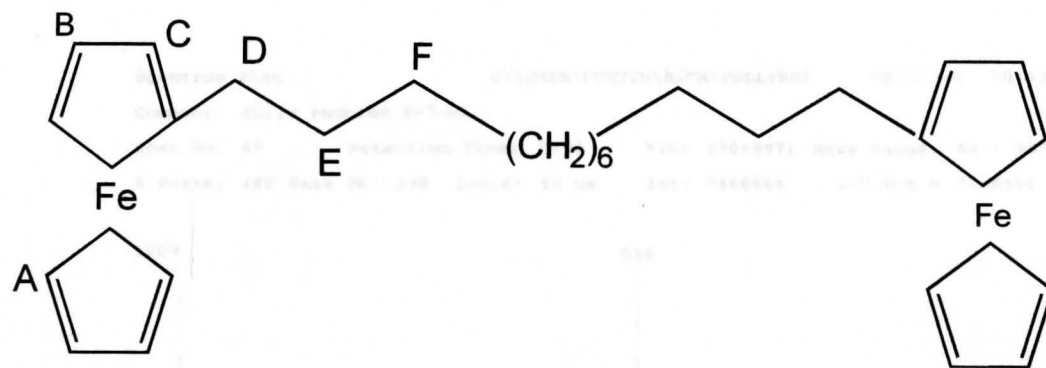


Figure 2.6: Mass spectrum of 1,12-diferrocenyldodecane

Figure 2.5: ¹H NMR spectrum of 1,12-diferrocenyldodecane

Spectrum Plot C:\USER\CURTIN\RICK\FULLYRE2 08/07/01 18:12:23
Comment: fully reduced 8-7-01
Scan No: 48 Retention Time: 0:51 RIC: 33849971 Mass Range: 50 - 990
Peaks: 480 Base Pk: 538 Ioniz: 59 us Int: 7466484 100.00% = 7466484

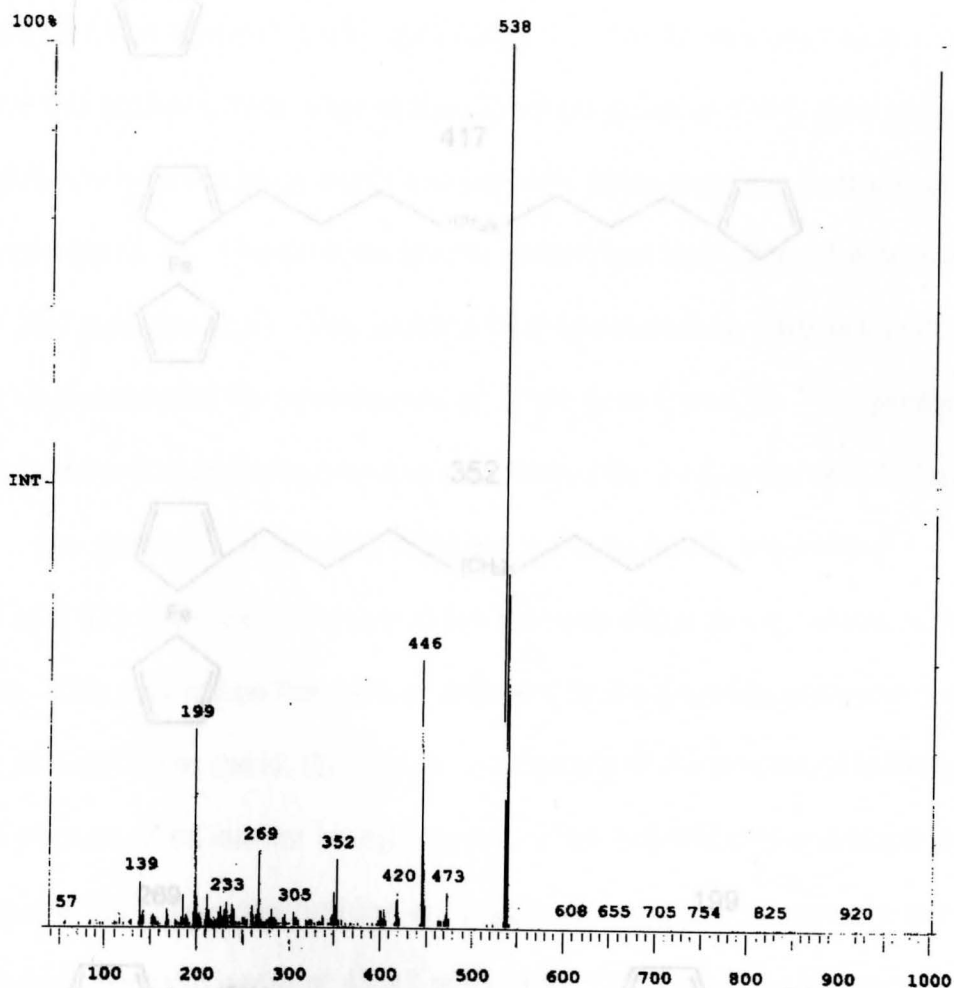


Figure 2.6: Mass spectrum of 1,12-diferrocenyldodecane

Figure 2.7: Major fragments (m/z) of 1,12-diferrocenyldodecane mass spectrum

2.3.3 Characterization of 1,12-diferrocenyldodecane

The ^1H NMR of the aromatic region (Figure 2.9) shows the multiplets of protons on carbon 1 and 12 of the 1,12-diferrocenyldodecane chain at 1.224 ppm (peak F). The protons on the first carbon from the bromide on the five carbon alkane chain occur at 1.401 ppm (peak O). On the bridging alkane chain the protons two carbons from each of the Cp rings occur at 1.483 ppm (peaks E, G). The protons on the alkane chain two carbons away from the carbonyl occur at 1.662 ppm (peak C). The protons on the carbon two away from the bromide occur at 1.660 ppm (peak P). The protons on the first carbon adjacent to the otherwise unsubstituted ferrocene occur at 2.194 ppm (peak D). The protons on the carbon next to the pentane bromide substituted Cp ring occur at 2.321 ppm (peak H). The protons on the other substituted Cp ring are shifted downfield at 2.673 ppm (peak M) due to the electron withdrawing nature of this substituent. The protons on the carbon adjacent to the bromide are even further downfield at 3.407 ppm (peak Q). Some broadening of the spectrum is likely due to a small amount of an isomer being present. The ^1H NMR of the ferrocene region (Figure 2.9) shows the protons on the top Cp ring opposite the bromide substituted Cp ring at 4.027 ppm (peak B). The other two protons on this ring occur at 4.039 ppm (peak B). The signal at 4.039 ppm (peaks A, L) indicates the protons on each of the bottom Cp rings. The protons on the top disubstituted Cp ring that are adjacent to the 12 carbon alkane chain occur at 4.376 and 4.396 ppm (peaks I and J, respectively). Finally, the proton on the Cp ring adjacent to the carbonyl substituent is shifted downfield at 4.560

Figure 2.7: Major fragments (m/z) of 1,12-diferrocenyldodecane mass spectrum

2.3.3 Characterization of 6-(diferrocenyldodecanylcarbonyl)pentane bromide

The ^1H NMR of the aliphatic region (Figure 2.8) shows the methylene protons on carbons 3-10 in the center of the 12 carbon alkane chain at 1.224 ppm (peak F). The protons on the third carbon from the bromide on the five carbon alkane chain occur at 1.401 ppm (peak O). On the bridging alkane chain the protons two carbons from each of the Cp^- rings occur at 1.493 ppm (peaks E, G). The protons on the alkane chain two carbons away from the carbonyl occur at 1.682 ppm (peak N). The protons on the carbon two away from the bromide occur at 1.890 ppm (peak P). The protons on the first carbon adjacent to the otherwise un-substituted ferrocene occur at 2.194 ppm (peak D). The protons on the carbon next to the pentane bromide substituted Cp^- ring occur at 2.321 ppm (peak H). The protons immediately adjacent to the carbonyl are shifted downfield at 2.673 ppm (peak M) due to the electron withdrawing nature of this substituent. The protons on the carbon adjacent to the bromide are even further downfield at 3.407 ppm (peak Q). Some broadening of the spectrum is likely due to a small amount of an isomer being present. The ^1H NMR of the ferrocene region (Figure 2.9) shows the protons on the top Cp^- ring that is opposite the bromide substituted ring occur at 4.027 ppm (peak C). The other two protons on this ring occur at 4.039 ppm (peak B). The signal at 4.089 ppm (peaks A, L) indicates the protons on each of the bottom Cp^- rings. The protons on the top disubstituted Cp^- ring that are adjacent to the 12 carbon alkane chain occur at 4.376 and 4.396 ppm (peaks I and J, respectively). Finally, the proton on the Cp^- ring that is adjacent to the carbonyl substituent is shifted downfield at 4.660

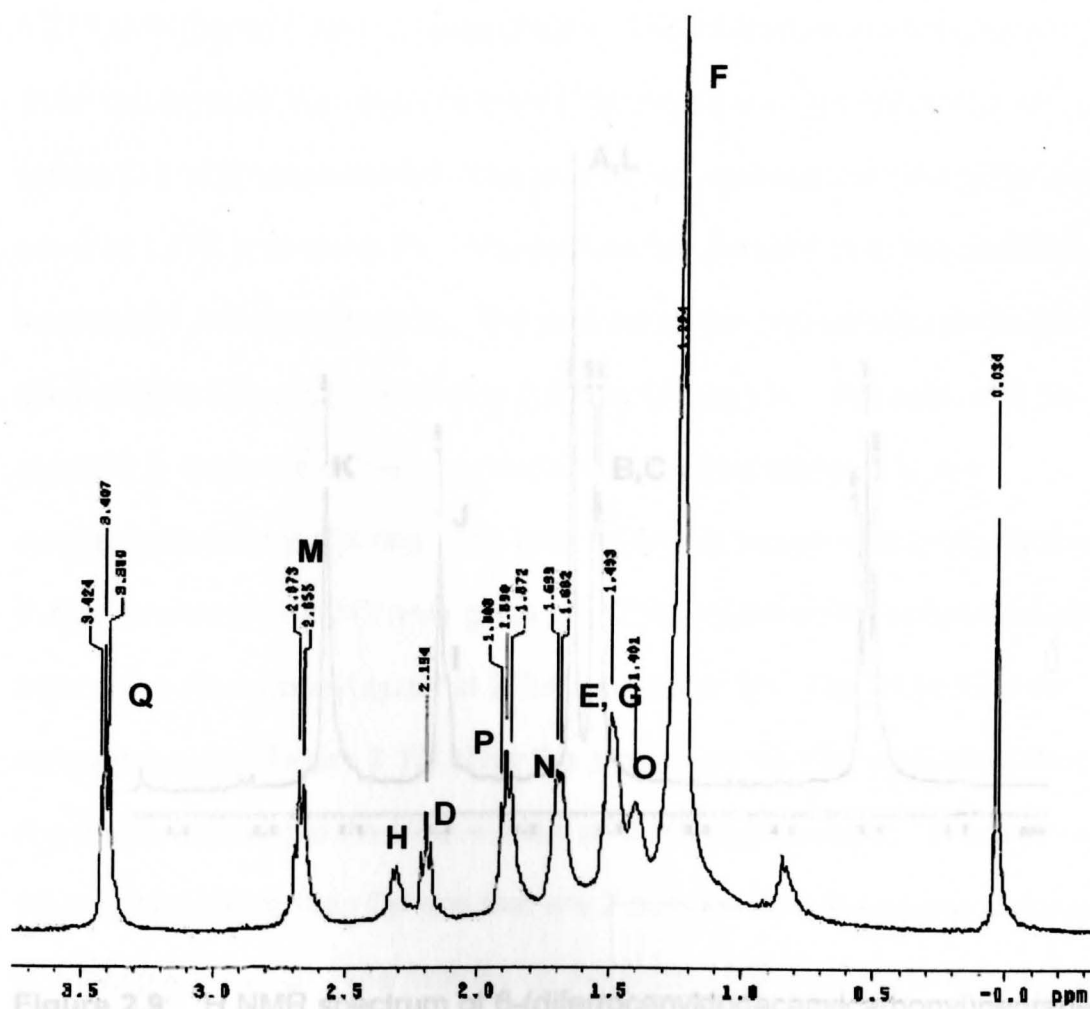
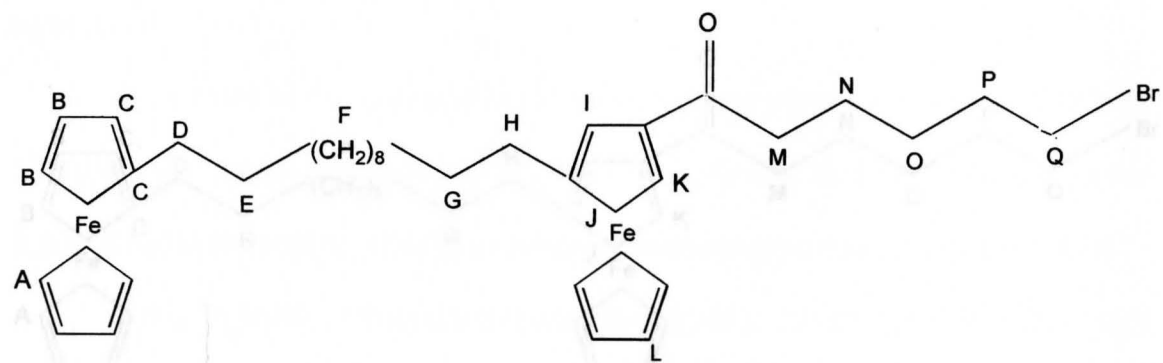
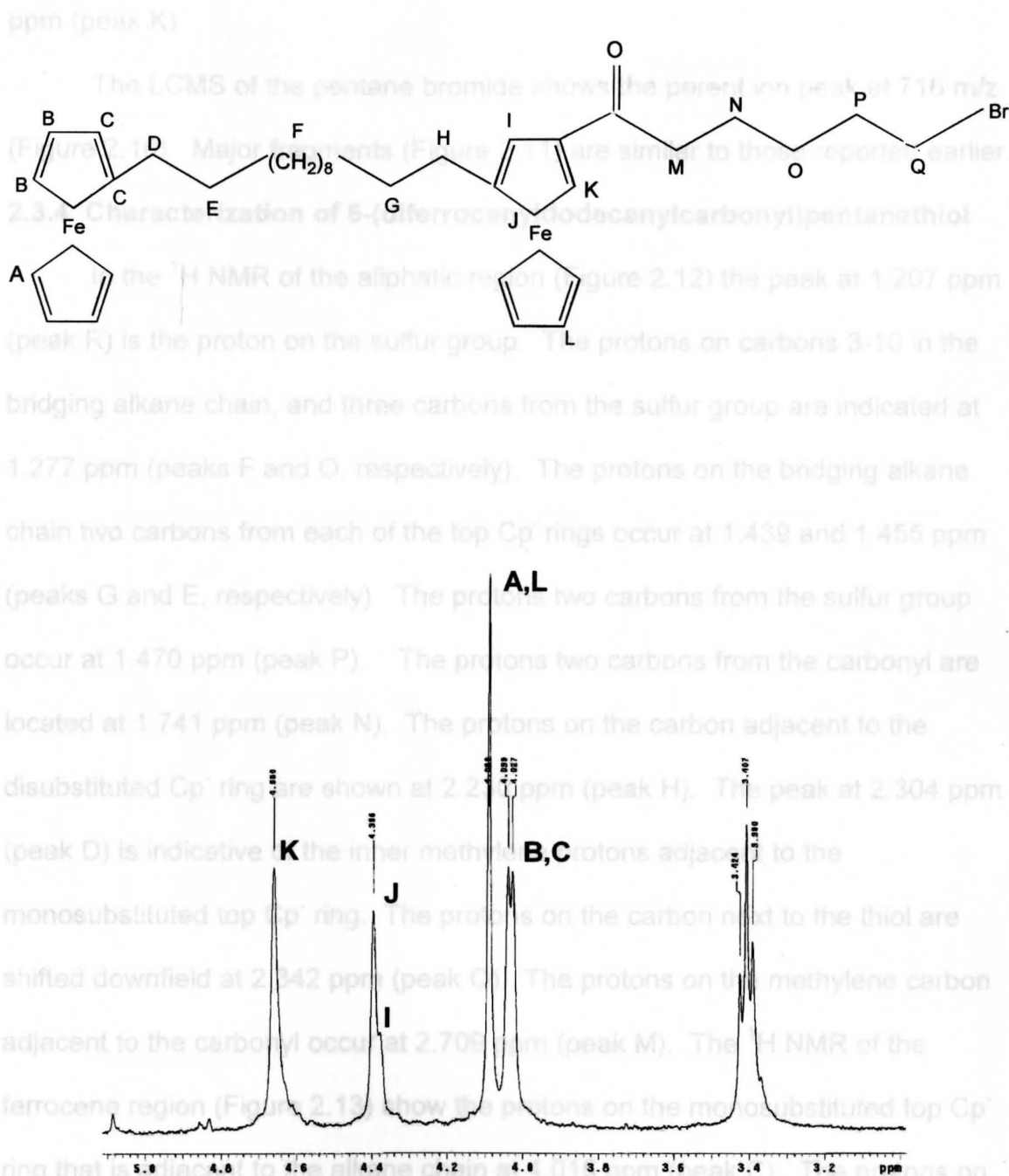


Figure 2.8: ^1H NMR spectrum of 6-(diferrocenyldodecanylcarbonyl) pentanebromide, aliphatic region



ppm (peak K).

The LCMS of the pentane bromide shows the parent ion peak at 716 m/z (Figure 2.10). Major fragments (Figure 2.11) are similar to those reported earlier.

2.3.4 Characterization of 6-(diferrocenyldodecanylcarbonyl)pentanethiol

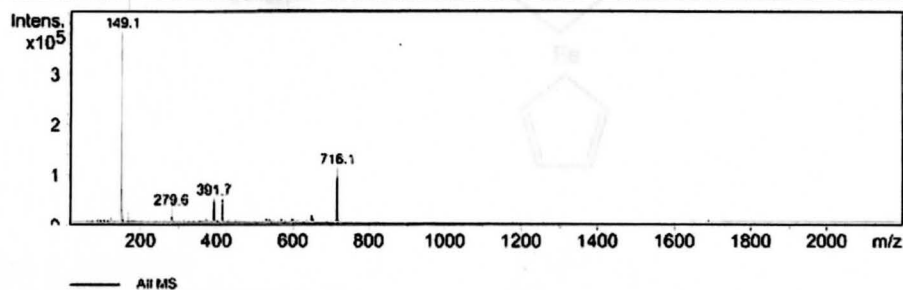
In the ^1H NMR of the aliphatic region (Figure 2.12) the peak at 1.207 ppm (peak R) is the proton on the sulfur group. The protons on carbons 3-10 in the bridging alkane chain, and three carbons from the sulfur group are indicated at 1.277 ppm (peaks F and O, respectively). The protons on the bridging alkane chain two carbons from each of the top Cp^- rings occur at 1.439 and 1.455 ppm (peaks G and E, respectively). The protons two carbons from the sulfur group occur at 1.470 ppm (peak P). The protons two carbons from the carbonyl are located at 1.741 ppm (peak N). The protons on the carbon adjacent to the disubstituted Cp^- ring are shown at 2.230 ppm (peak H). The peak at 2.304 ppm (peak D) is indicative of the inner methylene protons adjacent to the monosubstituted top Cp^- ring. The protons on the carbon next to the thiol are shifted downfield at 2.342 ppm (peak Q). The protons on the methylene carbon adjacent to the carbonyl occur at 2.709 ppm (peak M). The ^1H NMR of the ferrocene region (Figure 2.13) show the protons on the monosubstituted top Cp^- ring that is adjacent to the alkane chain at 4.015 ppm (peak C). The protons on the monosubstituted top Cp^- ring that are 2 carbons from the alkane chain occur at 4.049 ppm (peak B). The protons on the bottom Cp^- rings occur at 4.065 and 4.077 ppm (peaks A and L, respectively). The proton on the disubstituted Cp^- ring that is adjacent to the alkane chain occurs at 4.120 ppm (peak J). The proton on the top Cp^- ring between the alkane chains occur at 4.422 ppm (peak

Analysis Info

FileName	D:\Data\Porter\RP716A00.d\Analysis.yep	Print Date	Tuesday, 26 February 2002, 17:40
Acquisition Date	Tuesday, 02/26/02, 17:22:54	Operator	Administrator
Method	STD8Y.M	Instrument	Esquire-LC 00135
Comment	RP-1-716A		

Acquisition Parameter

Ion Source Type	ESI	Ion Polarity	Positive		
Mass Range Mode	Std/Normal	Scan Begin	15.00 m/z	Scan End	2200.00 m/z
Skim 1	52.0 Volt	Cap Exit Offset	77.0 Volt	Trap Drive	56.0
Accumulation Time	20000 μ s	Averages	10 Spectra		



Index	Mass	Intensity	Width	S/N
1	121.38	9662.00	0.54	37.04
2	149.12	422484.00	0.31	1619.62
3	149.91	37769.00	0.32	144.79
4	187.19	24015.00	0.43	92.05
5	279.55	29553.00	0.64	113.29
6	391.72	51181.00	0.75	156.21
7	392.83	21013.00	0.17	80.55
8	413.55	50817.00	0.72	194.81
9	649.15	13325.00	0.49	51.08
10	651.13	14244.00	0.45	54.61
11	714.61	93692.00	0.39	359.17
12	715.35	75498.00	0.38	289.43
13	716.15	119467.00	0.38	457.99
14	717.00	73809.00	0.37	282.95
15	717.98	23402.00	0.44	89.71

Bruker Daltonics DataAnalysis 2.0

Figure 2.10: Mass spectrum of 1,12-(diferrocenyldodecanylcarbonyl) pentanebromide

Figure 2.11: Major fragments (m/z) of 6-(diferrocenyldodecanylcarbonyl)pentane bromide mass spectrum

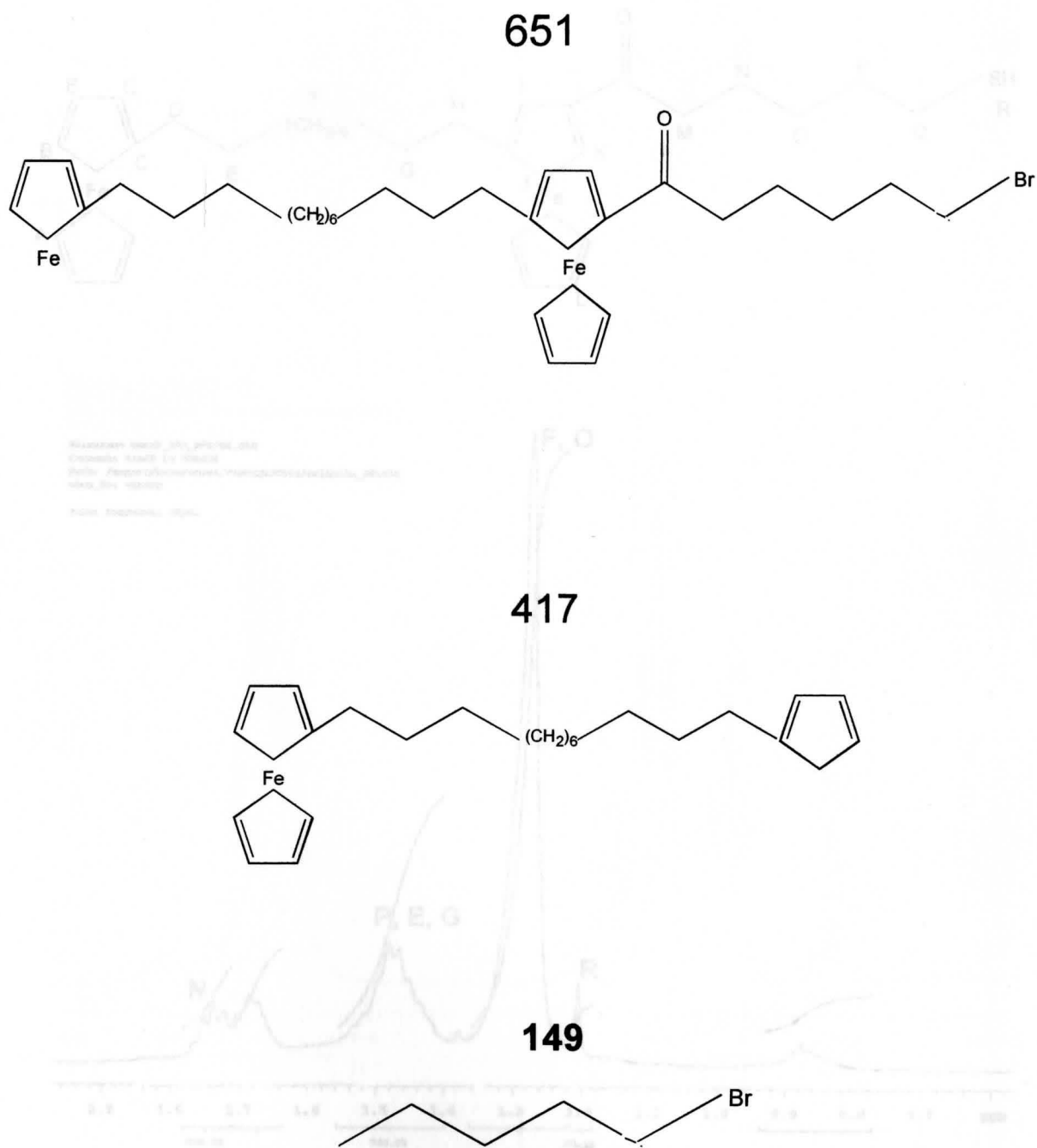
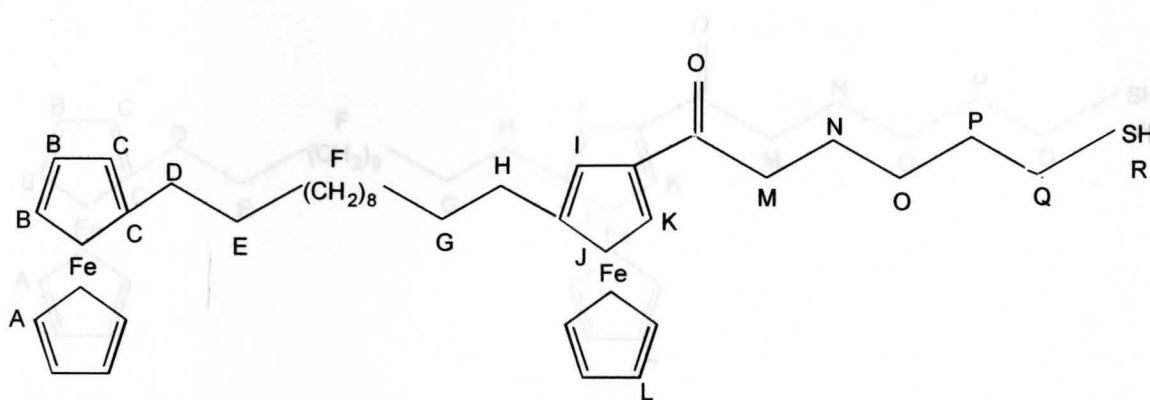


Figure 2.11: Major fragments (m/z) of 6-(diferrocenyldodecanylcarbonyl)pentane bromide mass spectrum



Filename: hmr1_001704_016
 Comment: hmr1 in 000015
 Path: /export/home/runner/vmruga/dota/olddata_001704
 Mrg_ID: 400499
 Pulse Sequence: zgpg1

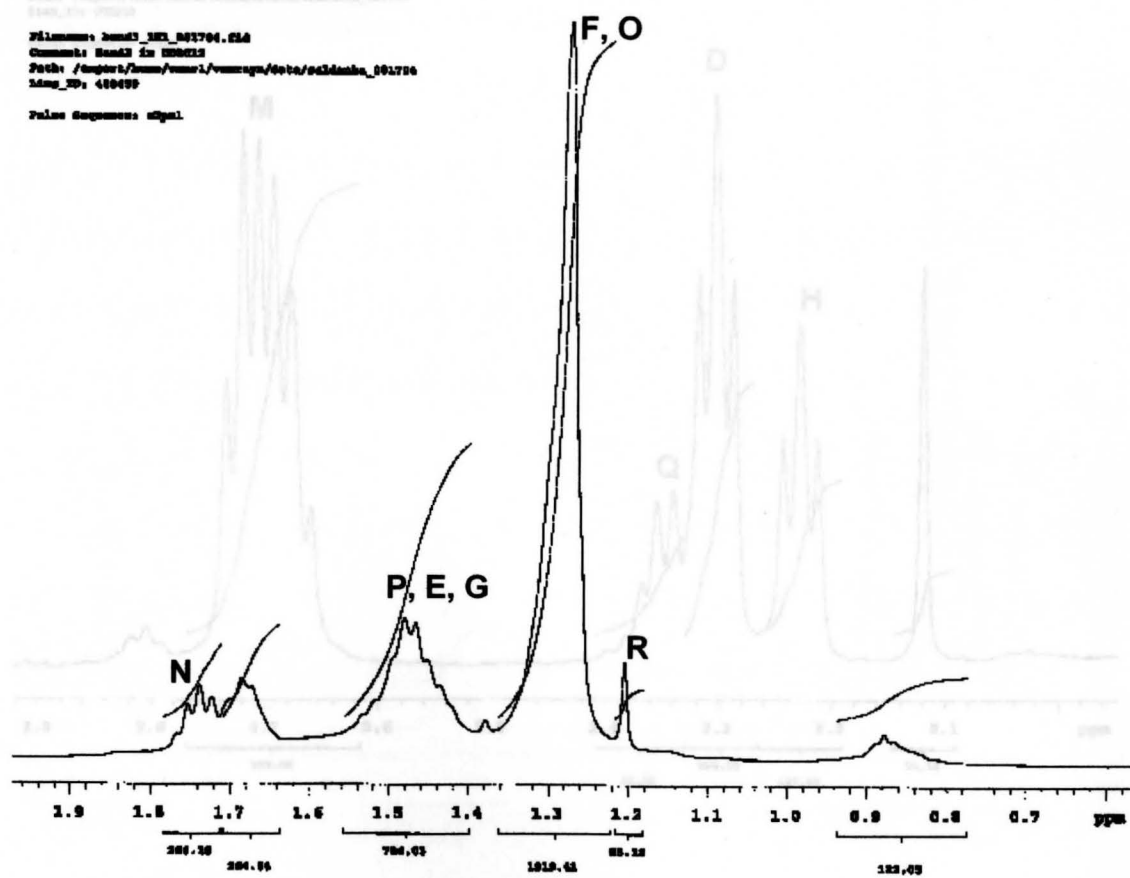
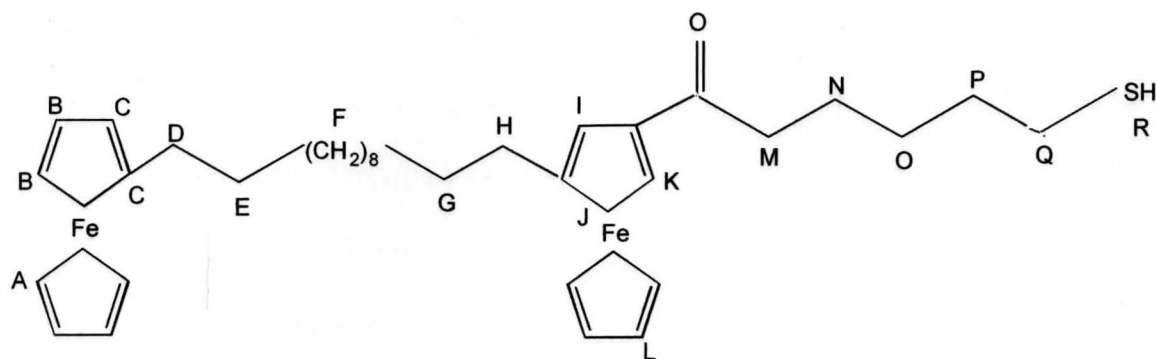


Figure 2.12 Continued: ¹H NMR of 6-(diferrocenyldodecanylcarbonyl)pentane

Figure 2.12: ¹H NMR of 6-(diferrocenyldodecanylcarbonyl)pentanethiol, aliphatic region



Filename: 000011_1H_001706.sia
 Comment: 1H NMR
 Path: /export/home/users/vmsrj/vmsrj/000011_1H_001706.sia
 Title: 000011
 Pulse Sequence: zgpg30

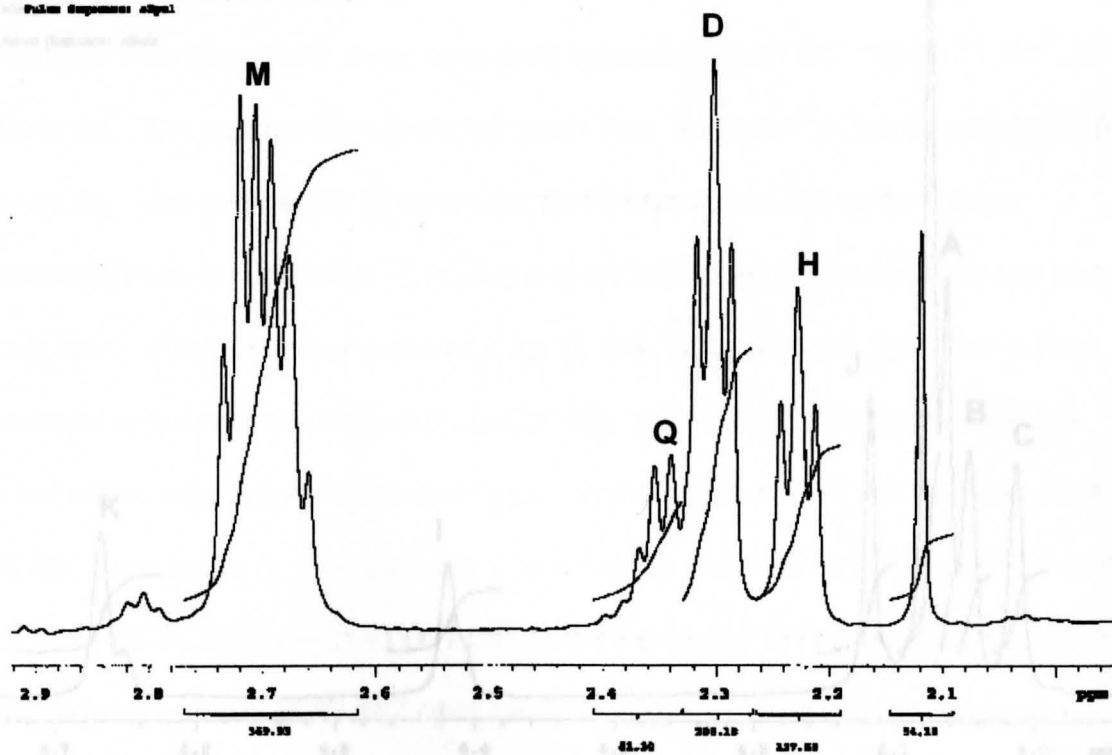
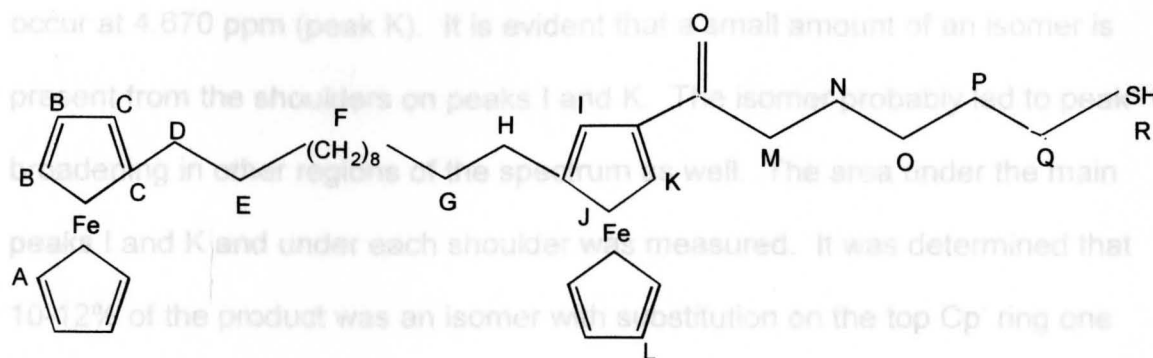


Figure 2.12 Continued: ^1H NMR of 6-(diferrocenyldodecanylcarbonyl)pentane thiol, aliphatic region

l). Finally, the proton adjacent to the carbonyl on the disubstituted top Cp' ring occur at 4.670 ppm (peak K). It is evident that a small amount of an isomer is present from the shoulders on peaks I and K. This isomer probably corresponds to the disubstituted top Cp' ring in the other region of the spectrum as well. The area under the main peak I and K and under each shoulder was measured. It was determined that 10.2% of the product was an isomer with substitution on the top Cp' ring one carbon away from the bridging alkane chain. Many attempts to separate the isomers chromatographically were unsuccessful.



Filename: head3_001704.fid
 Command: Bruker in CDCl3
 Path: /impech/chem/room1/runner/4/nto/so3dcaha_001704
 Idm_ID: 49048P

Pulse Sequence: zgpg30

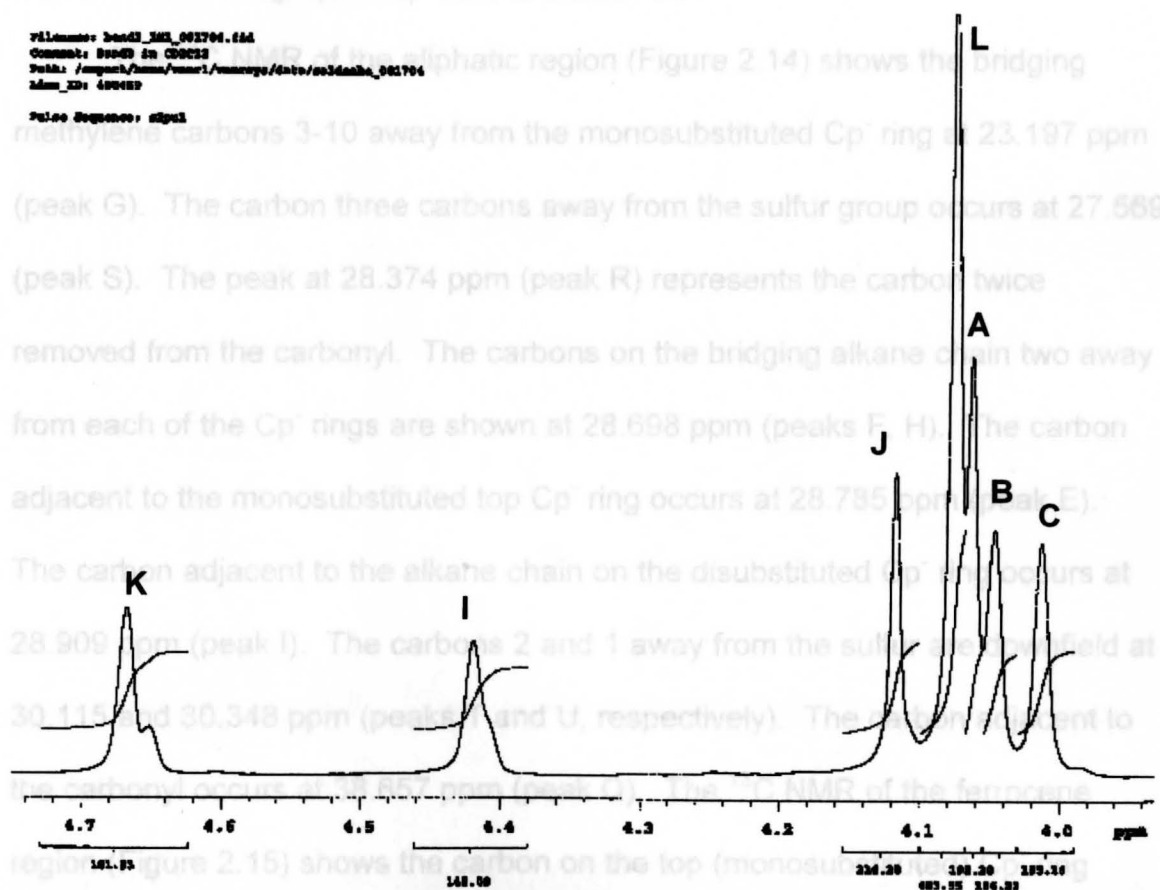


Figure 2.13: ¹H NMR of 6-(diferrocenyldodecanylcarbonyl)pentanethiol, ferrocene region

l). Finally, the proton adjacent to the carbonyl on the disubstituted top Cp⁻ ring occur at 4.670 ppm (peak K). It is evident that a small amount of an isomer is present from the shoulders on peaks I and K. The isomer probably led to peak broadening in other regions of the spectrum as well. The area under the main peaks I and K and under each shoulder was measured. It was determined that 10-12% of the product was an isomer with substitution on the top Cp⁻ ring one carbon away from the bridging alkane chain. Many attempts to separate the isomers chromatographically were unsuccessful.

The ¹³C NMR of the aliphatic region (Figure 2.14) shows the bridging methylene carbons 3-10 away from the monosubstituted Cp⁻ ring at 23.197 ppm (peak G). The carbon three carbons away from the sulfur group occurs at 27.569 (peak S). The peak at 28.374 ppm (peak R) represents the carbon twice removed from the carbonyl. The carbons on the bridging alkane chain two away from each of the Cp⁻ rings are shown at 28.698 ppm (peaks F, H). The carbon adjacent to the monosubstituted top Cp⁻ ring occurs at 28.785 ppm (peak E). The carbon adjacent to the alkane chain on the disubstituted Cp⁻ ring occurs at 28.909 ppm (peak I). The carbons 2 and 1 away from the sulfur are downfield at 30.115 and 30.348 ppm (peaks T and U, respectively). The carbon adjacent to the carbonyl occurs at 38.657 ppm (peak Q). The ¹³C NMR of the ferrocene region (Figure 2.15) shows the carbon on the top (monosubstituted) Cp⁻ ring where substitution of the inner alkane chain occurs is at 66.186 ppm (peak D). The carbons adjacent to the alkane chain on the top Cp⁻ ring are indicated by the signal at 67.279 ppm (peak C) (peak C). The carbons two away from the alkane chain are shown at 67.668 ppm (peak B). The carbons on the bottom Cp⁻ ring

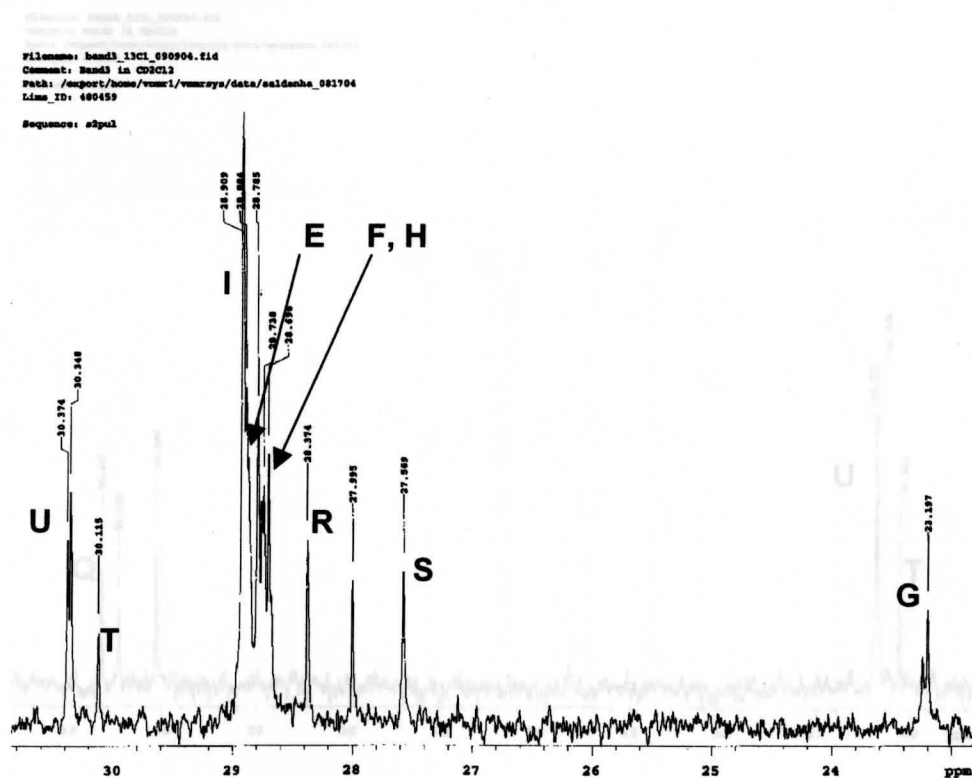
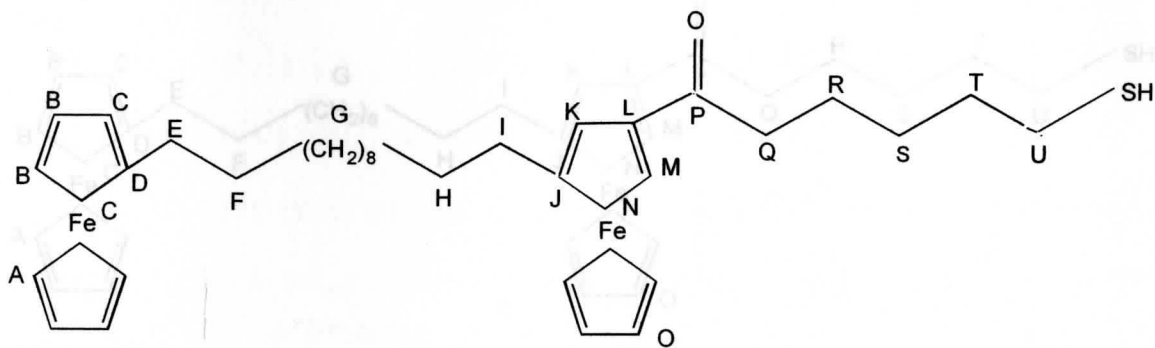


Figure 2.14: ^{13}C NMR of 6-(diferrocenyldodecanylcarbonyl)pentanethiol, aliphatic region

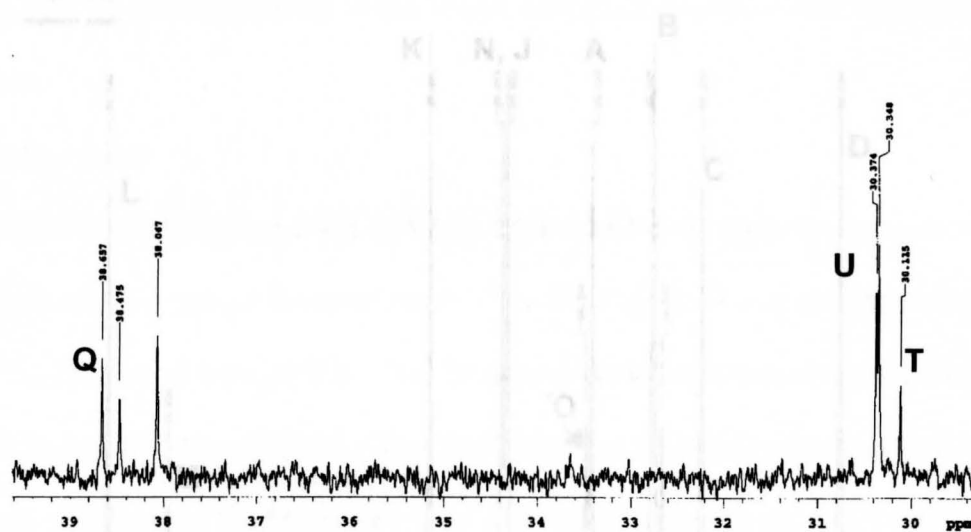
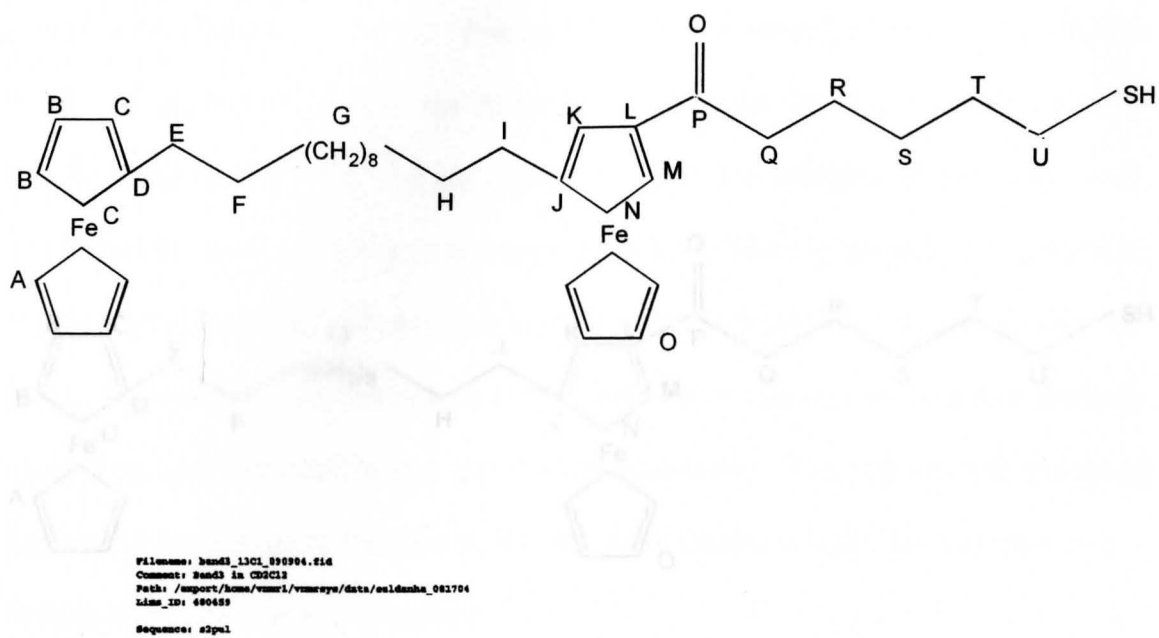
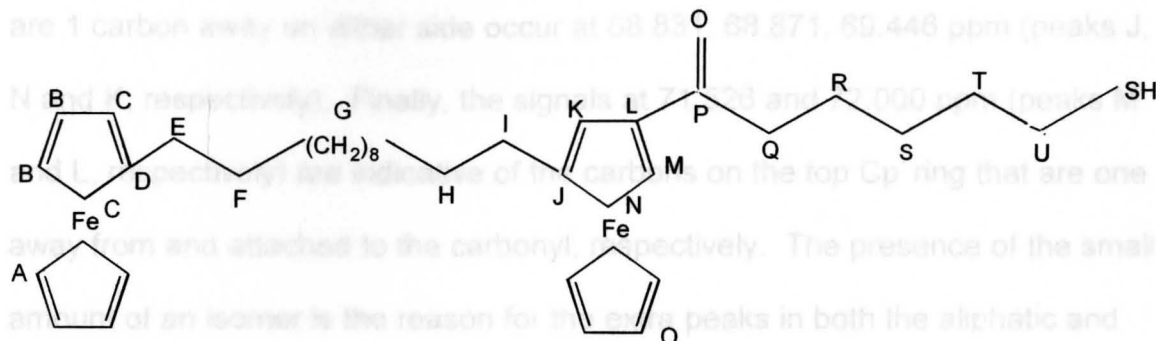


Figure 2.14 Continued: ^{13}C NMR of 6-(diferrocenyldodecanylcarbonyl)pentane thiol, aliphatic region

Figure 2.15. ^{13}C NMR of 6-(diferrocenyldodecanylcarbonyl)pentane thiol ferrocene region



Filename: hmad3_13C1_090904.f1d
 Comment: hmad3 in CDCl3
 Path: /export/home/vmsr1/vmsrva/data/anldmha_081704
 Ldas_ID: 680659
 Sequence: s2p01

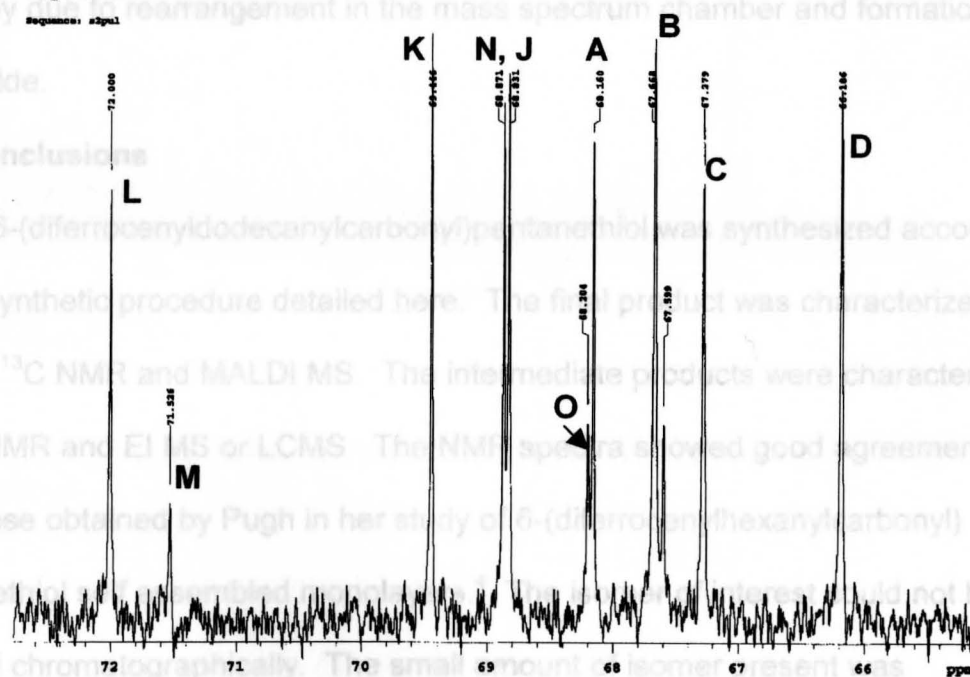


Figure 2.15: ^{13}C NMR of 6-(diferrocenyldodecanoyl)pentanethiol, ferrocene region

occur at 68.160 ppm (peak A). The carbons on the other bottom Cp⁻ ring, (below the di-substituted Cp⁻ ring) occur at 68.204 ppm (peak O). The carbons on the top disubstituted Cp⁻ ring that are substituted with the bridging alkane chain and are 1 carbon away on either side occur at 68.831, 68.871, 69.446 ppm (peaks J, N and K, respectively). Finally, the signals at 71.526 and 72.000 ppm (peaks M and L, respectively) are indicative of the carbons on the top Cp⁻ ring that are one away from and attached to the carbonyl, respectively. The presence of the small amount of an isomer is the reason for the extra peaks in both the aliphatic and ferrocene regions of the spectrum.

The MALDI MS (Figure 2.16) shows the parent ion at 1334.7 m/z, which is probably due to rearrangement in the mass spectrum chamber and formation of a disulfide.

2.4 Conclusions

6-(diferrocenyldodecanylcarbonyl)pentanethiol was synthesized according to the synthetic procedure detailed here. The final product was characterized by ¹H and ¹³C NMR and MALDI MS. The intermediate products were characterized by ¹H NMR and EI MS or LCMS. The NMR spectra showed good agreement with those obtained by Pugh in her study of 6-(diferrocenylhexanylcarbonyl)pentanethiol self assembled monolayers.⁴ The isomer of interest could not be isolated chromatographically. The small amount of isomer present was described, and may have led to some peak broadening in the spectra.

2.5 References

1. Chidsey, C. E. D. *Science* 1991, 251, 918
2. Chidsey, C. E. D.; Bertozzi, C. R.; Pulvinik, T. M.; Mujcsce, A. M. *J. Am. Chem. Soc.* 1990, 112, 4301-4306
3. Filler, W. J. Characterization of a Ferrocene Tagged Self-Assembled Alkanethiol Monolayers, M.S. Thesis, Temple University, August, 1996
4. Pugh, C. A. Synthesis and Electrochemical Characterization of Novel Bridged Ferrocene Tagged Alkanethiol Self-Assembled Monolayers, M.S. Thesis, Youngstown State University, May 2001
5. Mayers, V. Research in Progress
6. Creager, S.E.; Rowe, G.K. *J. Electroanal. Chem.* 1997, 420, 291-299
7. Wickman, J.J.; Ofer, D.; Zou, C.; Wrighton, M.S.; Leibins, P.E.; Whitesides, G.M. *J. Am. Chem. Soc.* 1991, 113, 1128-1132

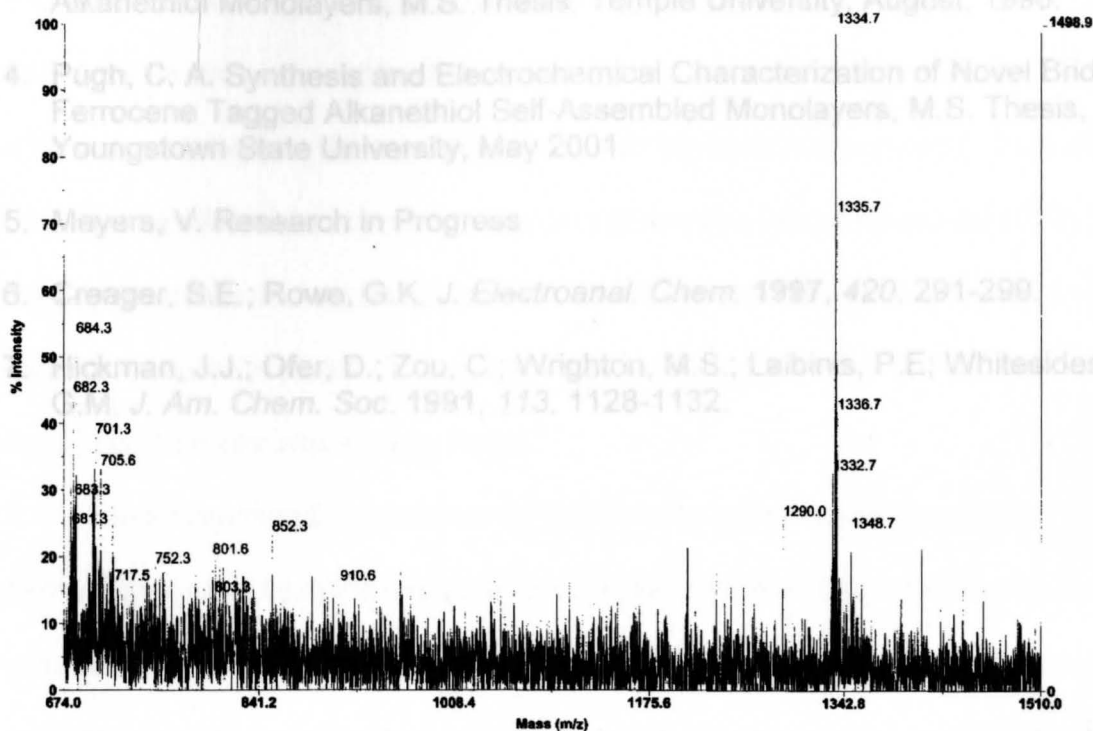


Figure 2.16: MALDI mass spectrum of 6-(diferrocenyldodecanylcarbonyl) pentanethiol

2.5 References

1. Chidsey, C. E. D. *Science* **1991**, *251*, 919.
2. Chidsey, C. E. D.; Bertozzi, C. R.; Putvinski, T. M.; Majsce, A. M. *J. Am. Chem. Soc.* **1990**, *112*, 4301-4306.
3. Filler, W. J. Characterization of Diferrocene Tagged Self-Assembled Alkanethiol Monolayers, M.S. Thesis, Temple University, August, 1996.
4. Pugh, C. A. Synthesis and Electrochemical Characterization of Novel Bridged Ferrocene Tagged Alkanethiol Self-Assembled Monolayers, M.S. Thesis, Youngstown State University, May 2001.
5. Meyers, V. Research in Progress
6. Creager, S.E.; Rowe, G.K. *J. Electroanal. Chem.* **1997**, *420*, 291-299.
7. Hickman, J.J.; Ofer, D.; Zou, C.; Wrighton, M.S.; Laibinis, P.E; Whitesides, G.M. *J. Am. Chem. Soc.* **1991**, *113*, 1128-1132.

Self-assembled monolayers of 6-(diferrocenyldodecarycarbonyl) pentanethiol on polycrystalline gold electrodes were also characterized by cyclic voltammetry. The full width at half maximum values (FWHM), ΔE_p 's, formal potentials, degree of chemical and electrochemical reversibility, and relative surface coverages were determined and evaluated for the monolayers. The results obtained are compared to those of Chidsey², Filler³, Pugh⁴ and Lewis⁴.

3.2 Chemicals

Perchloric acid (Fisher ACS Certified, 74%) was used as received. Acetonitrile (Fisher HPLC Grade, 99.9%) and methylene chloride (Fisher ACS Certified, 99.9%) were distilled over CaH_2 (Acros, 93%) and used immediately. Tetra-*n*-butylammonium perchlorate (TBAP, Fluka, 98%) was recrystallized three times from ethanol and dried under vacuum.

CHAPTER THREE

ELECTROCHEMISTRY

3.1 Introduction

The synthesis of 6-(diferrocenyldodecanylcarbonyl)pentanethiol was completed according to the protocol detailed in the previous chapter. Two intermediate products; 1,12-diferrocenyldodecane-1,12-dione and 1,12-diferrocenyldodecane were analyzed via solution cyclic voltammetry. This was done to characterize each compound and determine formal potentials (E° 's), ΔE_p values, chemical and electrochemical reversibility and diffusion control of the electron transfer process. The values obtained from the experiments are compared to those reported by Pugh.¹

Self-assembled monolayers of 6-(diferrocenyldodecanylcarbonyl)pentanethiol on polycrystalline gold electrodes were also characterized by cyclic voltammetry. The full width at half maximum values (FWHM), ΔE_p 's, formal potentials, degree of chemical and electrochemical reversibility, and relative surface coverages were determined and evaluated for the monolayers. The results obtained are compared to those of Chidsey², Filler³, Pugh¹ and Lewis.⁴

3.2 Chemicals

Perchloric acid (Fisher ACS Certified, 74%) was used as received. Acetonitrile (Fisher HPLC Grade, 99.9%) and methylene chloride (Fisher ACS Certified, 99.9%) were distilled over CaH_2 (Acros, 93%) and used immediately. Tetra-*n*-butylammonium perchlorate (TBAP, Fluka, 98%) was recrystallized three times from ethanol and dried under vacuum.

3.3 Instrumentation

Cyclic voltammetry experiments were conducted with a Bioanalytical Systems (BAS) 100B potentiostat. For the solution voltammetry, a 1.6 mm diameter platinum disc working electrode, platinum wire counter electrode and non-aqueous Ag/AgNO₃ reference electrode were used. In the monolayer voltammetry experiments, a 1.6 mm diameter gold disc electrode, platinum wire counter electrode, and an aqueous Ag/AgCl reference electrode were used. The platinum, gold disc and reference electrodes were purchased from BAS. All experiments were conducted in a single compartment electrochemical cell. No attempt was made to remove oxygen from the solutions.

3.4 Experimental

3.4.1 Electrode Preparation

The platinum disc electrodes used in the solution voltammetry experiments were polished for 15 minutes on a flock twill cloth coated with a 1 μm Al₂O₃ / de-ionized water slurry.¹ The electrodes were then rinsed with de-ionized water, ultrasonically cleaned in de-ionized water for 15 minutes and rinsed again with acetonitrile before use.

The gold disc electrodes used in the monolayer voltammetry experiments were used as received and ultrasonically cleaned for 20 minutes in de-ionized water. The electrodes were electrochemically cleaned by immersing them in ~10 ml of a 1 M solution of aqueous HClO₄. Ag/AgCl reference and Pt wire counter electrodes were used and the gold disc working electrode was scanned from an initial potential of -1500 mV to a potential of 1500 mV at a scan rate of 250

mV/sec. Then the scan was reversed and scanned back to -1500 mV. This procedure was repeated ten times to ensure a fully reduced gold surface for adsorption of the alkanethiol. The electrodes were then evaluated by scanning from 0 to 700 mV, at which point the scan was reversed and scanned back to 0 mV at a scan rate of 50 mV/sec. This was done to make sure no impurities were present on the electrode or in the electrolyte. The electrodes were then rinsed in de-ionized water and CH_2Cl_2 . Following cleaning, the electrodes were each immersed in ~ 5 ml of coating solution containing 1 mM 6-(diferrocenyldodecanylcarbonyl)pentanethiol dissolved in CH_2Cl_2 . Electrodes designated E11 and E12 were immersed for approximately 18 hours in the stirred coating solutions. The electrodes were removed from the coating solutions, rinsed again in CH_2Cl_2 and 1.0 M HClO_4 (aq) and were used immediately in the cyclic voltammetry experiments.

3.4.2 Solution Voltammetry

Solution cyclic voltammetry was conducted in 1 mM solutions of the analyte with 0.1 M TBAP in acetonitrile. Approximately 10 ml of the solutions were used. The formal potentials were determined. The ratio of peak currents and difference in peak potentials as a function of scan rate for each wave were determined to assess chemical and electrochemical reversibility. Diffusion control of the electron transfer was evaluated by plotting the anodic peak currents versus the square root of the scan rate.

3.4.3 Monolayer Voltammetry

Each monolayer coated gold electrode was electrochemically evaluated in

1 M aqueous HClO₄ solution. The ratio of peak currents ($i_{p,a}/i_{p,c}$), formal potentials (E° 's), and difference in peak potentials (ΔE_p) were determined for each wave, at each scan rate. The peak areas were calculated for each wave to determine the surface coverages^{1,5} (corrected for surface roughness) by using the formula:

$$\Gamma = (\text{Area of peak}) / 0.0402 \text{ cm}^2 n F \nu$$

Where: n is the number of electrons transferred, F is Faradays constant (96,486 coulombs per mole of electrons), and ν is the scan rate in volts per second. The degree of ordering was assessed by determining the full width at half-maximum values (FWHM) for the voltammetric waves, and the heterogenous electron transfer rate constant for each electron transfer. The relationship between anodic peak currents and scan rate was determined to establish the presence of a surface confined species. The values obtained here are compared to values obtained by Pugh¹ & Lewis⁴ in their studies of 6-(diferrocenylohexanecarbonyl) pentanethiol monolayers, and Filler³ in his study of diferrocenylethane-tagged C-6 monolayers, where applicable.

3.5 Results / Discussion

3.5.1 Solution Voltammetry

A solution of 1,12-diferrocenyldodecane-1,12-dione was evaluated at scan rates of 25, 50, 75, and 100 to 500 mv/sec in 50 mv/sec increments and from 500 to 1,000 mv/sec in 100 mv/sec increments. A cyclic voltammetric comparison of scan rates at 50, 100 and 150 mv/sec is shown in Figure 3.1. The voltammograms display a single, two electron oxidation with an E° of 266 mV,

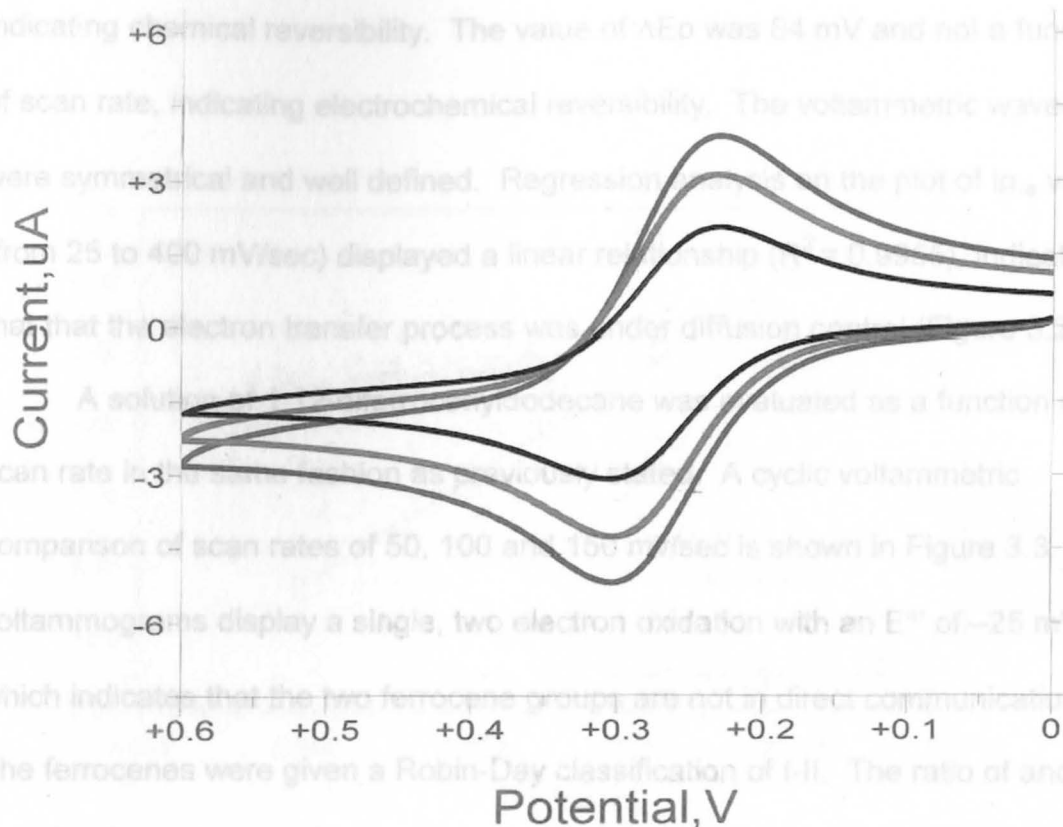


Figure 3.1: Cyclic voltammograms of 1 mM 1,12-diferrocenyldodecane-1,12-dione in 0.1 M TBAP in CH_3CN . Platinum working and counter electrode, Ag/AgNO_3 reference electrode, 25°C . Blue = 150 mV/sec, red = 100 mV/sec, black = 50 mV/sec.

The difference in formal potentials between 1,12-diferrocenyldodecane-1,12-dione, and the fully reduced 1,12-diferrocenyldodecane is due to removal of

which indicates that the two ferrocene groups are not in direct communication. The ferrocenes were given a Robin-Day classification of I-II. The ratio of anodic to cathodic peak currents was essentially one and not dependent on scan rate, indicating chemical reversibility. The value of ΔE_p was 84 mV and not a function of scan rate, indicating electrochemical reversibility. The voltammetric waves were symmetrical and well defined. Regression analysis on the plot of $i_{p,a}$ vs. $v^{1/2}$ (from 25 to 400 mV/sec) displayed a linear relationship ($R^2 = 0.9955$), indicating that the electron transfer process was under diffusion control (Figure 3.2).

A solution of 1,12-diferrocenyldodecane was evaluated as a function of scan rate in the same fashion as previously stated. A cyclic voltammetric comparison of scan rates of 50, 100 and 150 mv/sec is shown in Figure 3.3. The voltammograms display a single, two electron oxidation with an E° of -25 mV, which indicates that the two ferrocene groups are not in direct communication. The ferrocenes were given a Robin-Day classification of I-II. The ratio of anodic to cathodic peak currents was essentially one and not dependent on scan rate, indicating chemical reversibility. The ΔE_p was 87 mV and not a function of scan rate, indicating electrochemical reversibility. The voltammetric waves were symmetrical and well defined. Regression analysis on the plot of $i_{p,a}$ vs. $v^{1/2}$ (from 25 to 400 mV/sec) displayed a linear relationship ($R^2 = 0.9984$). This indicated that the electron transfer process was under diffusion control (Figure 3.4).

The difference in formal potentials between 1,12-diferrocenyldodecane-1,12-dione, and the fully reduced 1,12-diferrocenyldodecane is due to removal of

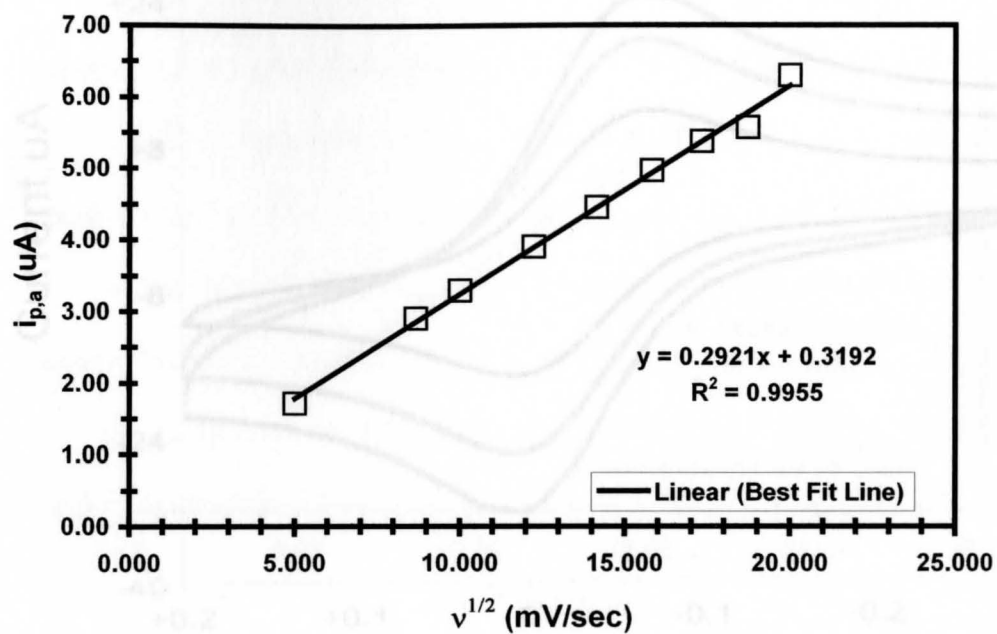


Figure 3.2: Anodic peak currents ($i_{p,a}$) vs. $v^{1/2}$ for 1,12-diferrocenyldodecane-1,12-dione

Figure 3.3: Cyclic voltammograms of 1 mM 1,12-diferrocenyldodecane in 0.1 M TBAP in CH_3CN . Platinum working and counter electrode, Ag/AgNO_3 reference electrode, 25°C. Blue = 150 mV/sec , red = 100 mV/sec , black = 50 mV/sec .

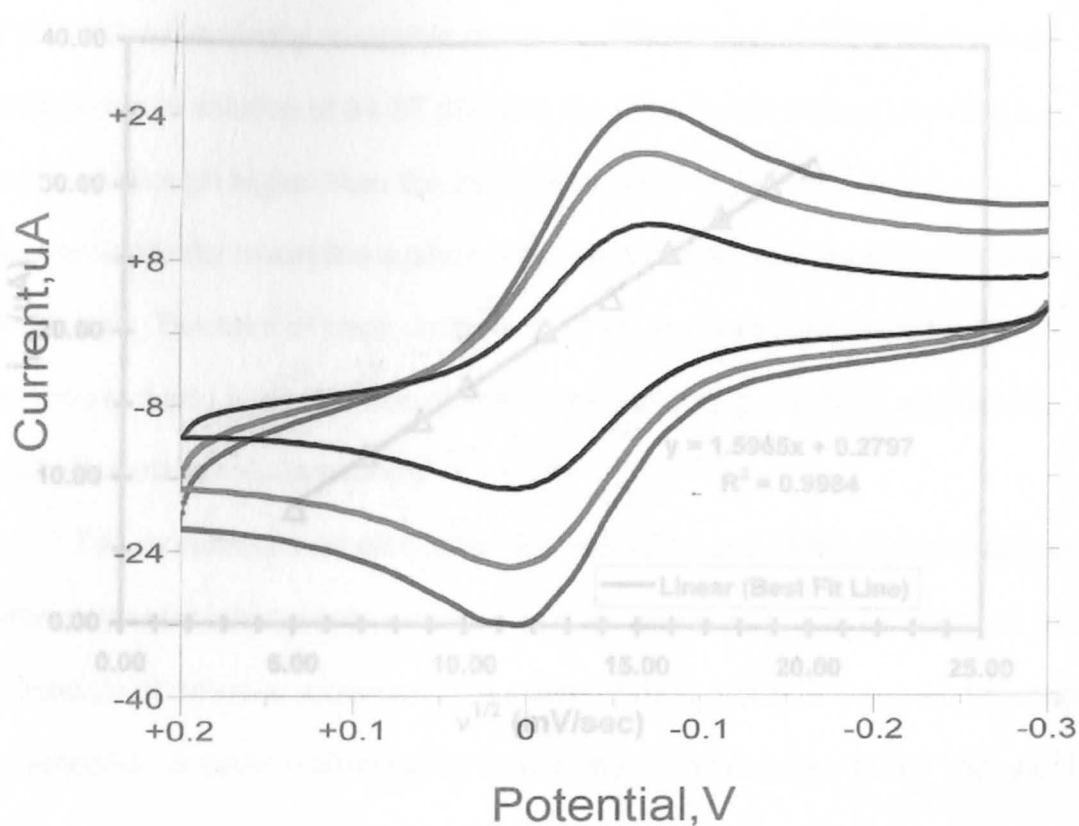


Figure 3.4: Anodic peak currents ($i_{p,a}$) vs. $v^{1/2}$ for 1,12-diferrocenyldodecane

Figure 3.3: Cyclic voltammograms of 1 mM 1,12-diferrocenyldodecane in 0.1 M TBAP in CH_3CN . Platinum working and counter electrode, Ag/AgNO_3 reference electrode, 25°C. Blue = 150 mV/sec, red = 100 mV/sec, black = 50 mV/sec.

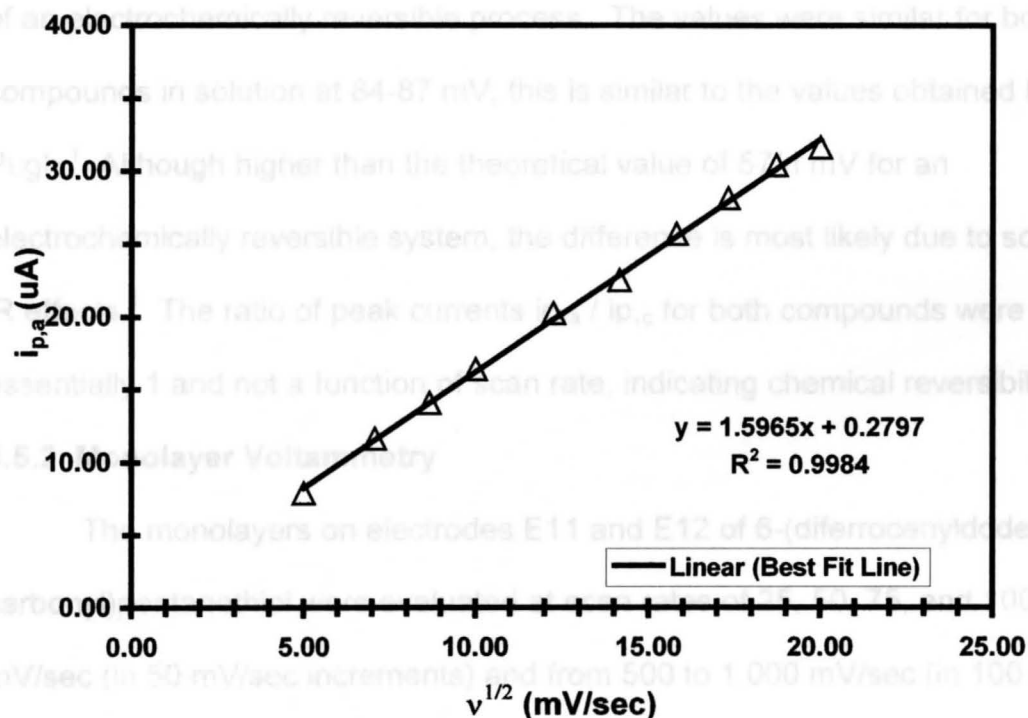
the electron withdrawing carbonyl substituents.¹ It is well documented that carbonyl substitution of ferrocene compounds shifts the formal potentials to more anodic values versus ferrocene, whereas electron donating alkyl groups have the opposite effect.^{1,3} The ΔE_p values were independent of scan rate and indicative

of an electrochemically reversible process. The values were similar for both compounds in solution at 84-87 mV, this is similar to the values obtained by Pugh¹ though higher than the theoretical value of 57 mV for an electrochemically reversible system, the difference is most likely due to solution resistance. The ratio of peak currents ($i_{p,c}/i_{p,a}$) for both compounds were essentially 1 and not a function of scan rate, indicating chemical reversibility.

3.5.2. Cyclic Voltammetry
The monolayers on electrodes E11 and E12 of 6-(diferrocenyldodecanyl) carbonyl dodecane were studied by cyclic voltammetry at scan rates of 100 to 500 mV/sec (in 50 mV/sec increments) and from 500 to 1 000 mV/sec (in 100 mV/sec increments). A cyclic voltammetric comparison of scan rates at 50, 100 and 150 mV/sec is shown in Figures 3.5 and 3.6 for monolayers on electrodes E11 and

Figure 3.4: Anodic peak currents ($i_{p,a}$) vs. $v^{1/2}$ for 1,12-diferrocenyl dodecane

The voltammograms for both of the electrodes exhibited remarkably similar behavior, with two single electron transfers, and similar values for most parameters. The first wave (outer ferrocenes) was very broad and poorly defined, while the second wave (inner ferrocenes) was very well defined. The voltammograms reported by Filler² in his study of diferrocenyldodecane-



the electron withdrawing carbonyl substituents.¹ It is well documented that carbonyl substitution of ferrocene compounds shifts the formal potentials to more anodic values versus ferrocene, whereas electron donating alkyl groups have the opposite effect.^{1,3} The ΔE_p values were independent of scan rate and indicative of an electrochemically reversible process. The values were similar for both compounds in solution at 84-87 mV, this is similar to the values obtained by Pugh.¹ Although higher than the theoretical value of $57/n$ mV for an electrochemically reversible system, the difference is most likely due to solution iR effects.¹ The ratio of peak currents $i_{p,a} / i_{p,c}$ for both compounds were essentially 1 and not a function of scan rate, indicating chemical reversibility.

3.5.2 Monolayer Voltammetry

The monolayers on electrodes E11 and E12 of 6-(diferrocenyldodecanyl carbonyl)pentanethiol were evaluated at scan rates of 25, 50, 75, and 100 to 500 mV/sec (in 50 mV/sec increments) and from 500 to 1,000 mV/sec (in 100 mV/sec increments). A cyclic voltammetric comparison of scan rates at 50, 100 and 150 mV/sec is shown in Figures 3.5 and 3.6 for monolayers on electrodes E11 and E12.

The voltammograms for both of the electrodes exhibited remarkably similar behavior, with two single electron transfers, and similar values for most parameters. The first wave (outer ferrocenes) was very broad and poorly defined, while the second wave (inner ferrocenes) was very well defined. The voltammograms reported by Filler³ in his study of diferrocenylethane-

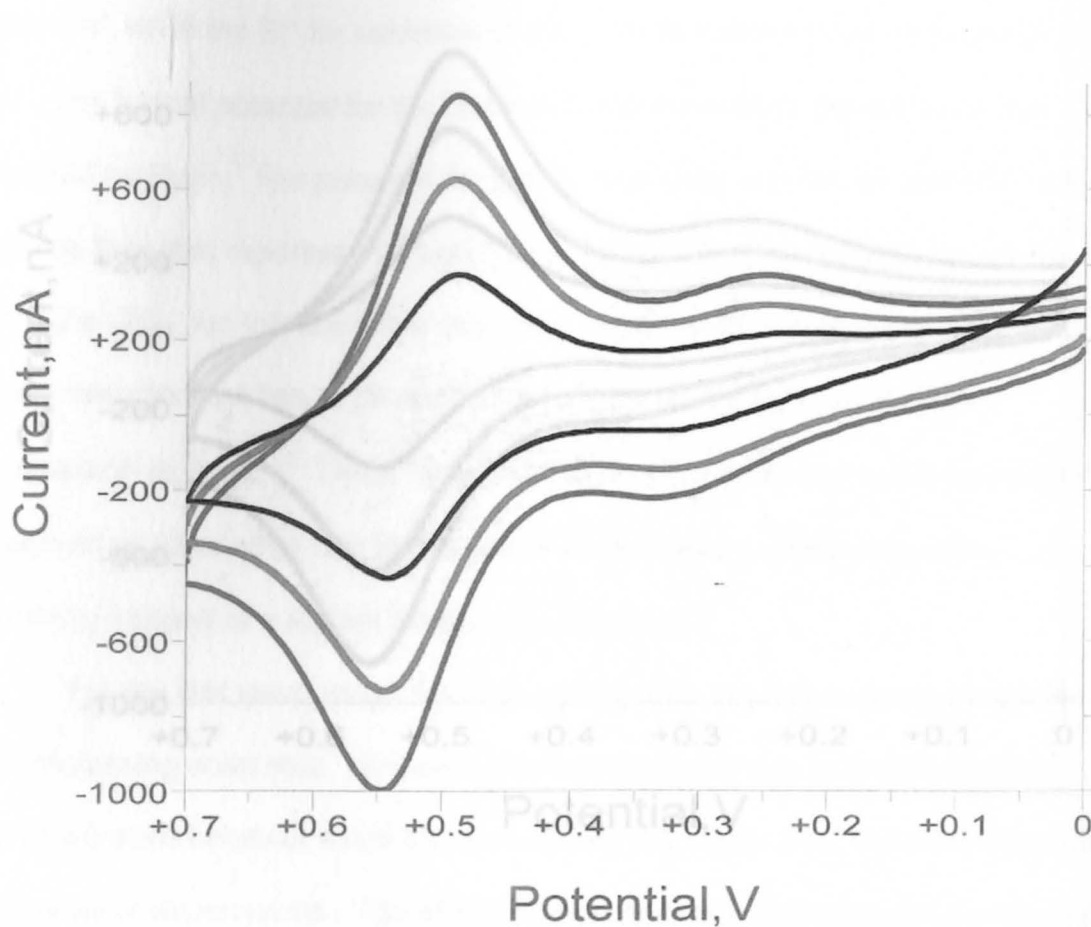


Figure 3.6: Cyclic voltammograms of a 6-(diferrocenyldodecanylcarbonyl) pentanethiol monolayer on electrode E12. Blue = 150 mV/sec, red = 100 mV/sec, black = 50 mV/sec.

Figure 3.5: Cyclic voltammograms of a 6-(diferrocenyldodecanylcarbonyl) pentanethiol monolayer on electrode E11. Blue = 150 mV/sec, red = 100 mV/sec, black = 50 mV/sec.

tagged C-6 monolayers and Pugh¹ in her study of 5-(diferrocenyldodecanylcarbonyl)pentanethiol monolayers displayed two well defined waves for both ferrocene groups.

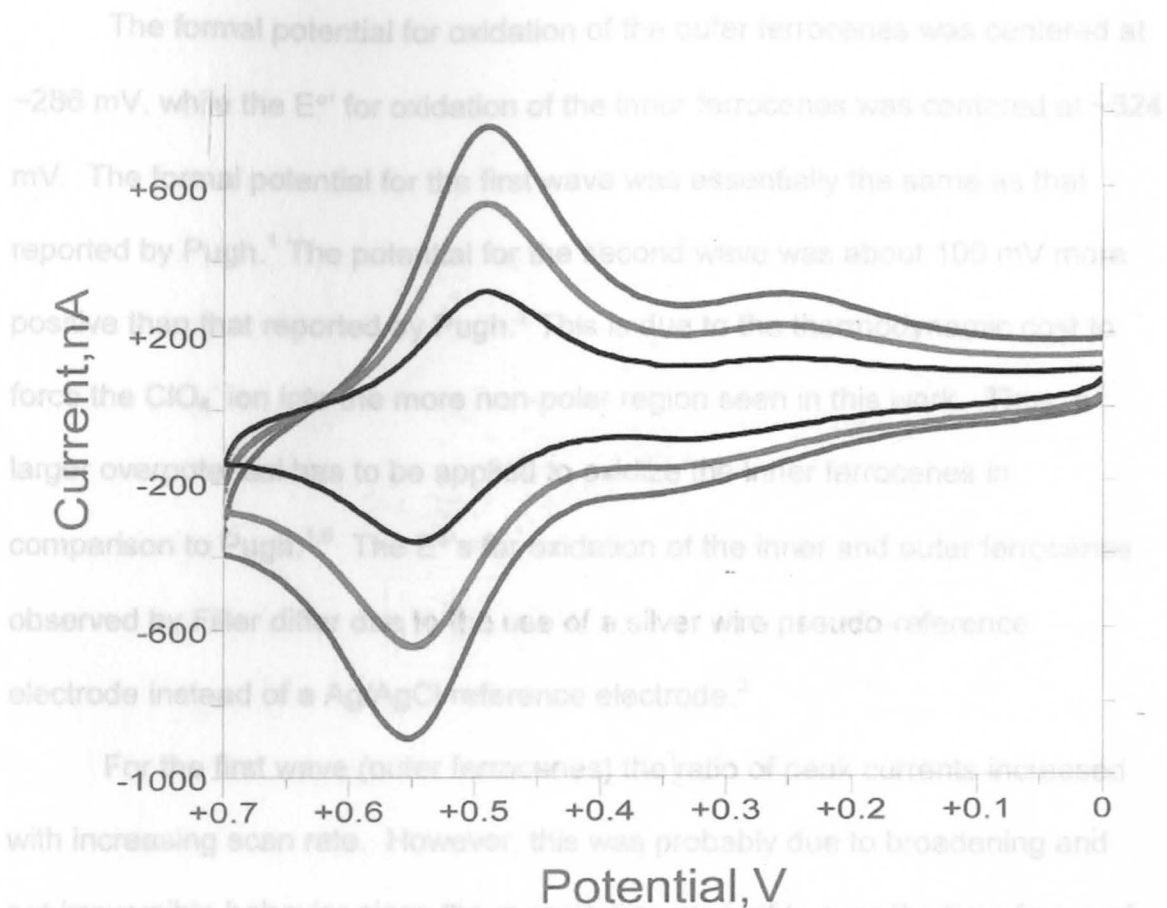


Figure 3.6: Cyclic voltammograms of a 6-(diferrocenyldodecanylcarbonyl) pentanethiol monolayer on electrode E12. Blue = 150 mV/sec, red = 100 mV/sec, black = 50 mV/sec.

For the first wave (outer ferrocenes) the ratio of peak currents increased with increasing scan rate. However, this was probably due to broadening and not irreversible behavior since the monolayers are stable over the time frame of the series of experiments. The effect of scan rate on broadening for a monolayer

The ΔE_p values for the first wave (outer ferrocenes) showed some slight fluctuations, but generally increased with increasing scan rate up to 500 mV/sec.

tagged C-6 monolayers and Pugh¹ in her study of 6-(diferrocenylohexanonyl)pentanethiol monolayers displayed four well-defined waves for both ferrocene groups.

The formal potential for oxidation of the outer ferrocenes was centered at ~286 mV, while the E° for oxidation of the inner ferrocenes was centered at ~524 mV. The formal potential for the first wave was essentially the same as that reported by Pugh.¹ The potential for the second wave was about 100 mV more positive than that reported by Pugh.¹ This is due to the thermodynamic cost to force the ClO_4^- ion into the more non-polar region seen in this work. Thus, a larger overpotential has to be applied to oxidize the inner ferrocenes in comparison to Pugh.^{1,6} The E° 's for oxidation of the inner and outer ferrocenes observed by Filler differ due to the use of a silver wire pseudo-reference electrode instead of a Ag/AgCl reference electrode.³

For the first wave (outer ferrocenes) the ratio of peak currents increased with increasing scan rate. However, this was probably due to broadening and not irreversible behavior since the monolayers are stable over the time frame of the series of experiments. The effect of scan rate on broadening for a monolayer at 100 and 400 mV/sec are evident in Figure 3.7. For the second (inner ferrocenes) wave the peak current ratio was ~1 indicating a chemically reversible process. This agrees with Pugh's¹ and Filler's³ data in that both the inner and outer ferrocene waves exhibited chemical reversibility.

The ΔE_p values for the first wave (outer ferrocenes) showed some slight fluctuations, but generally increased with increasing scan rate up to 500 mV/sec.

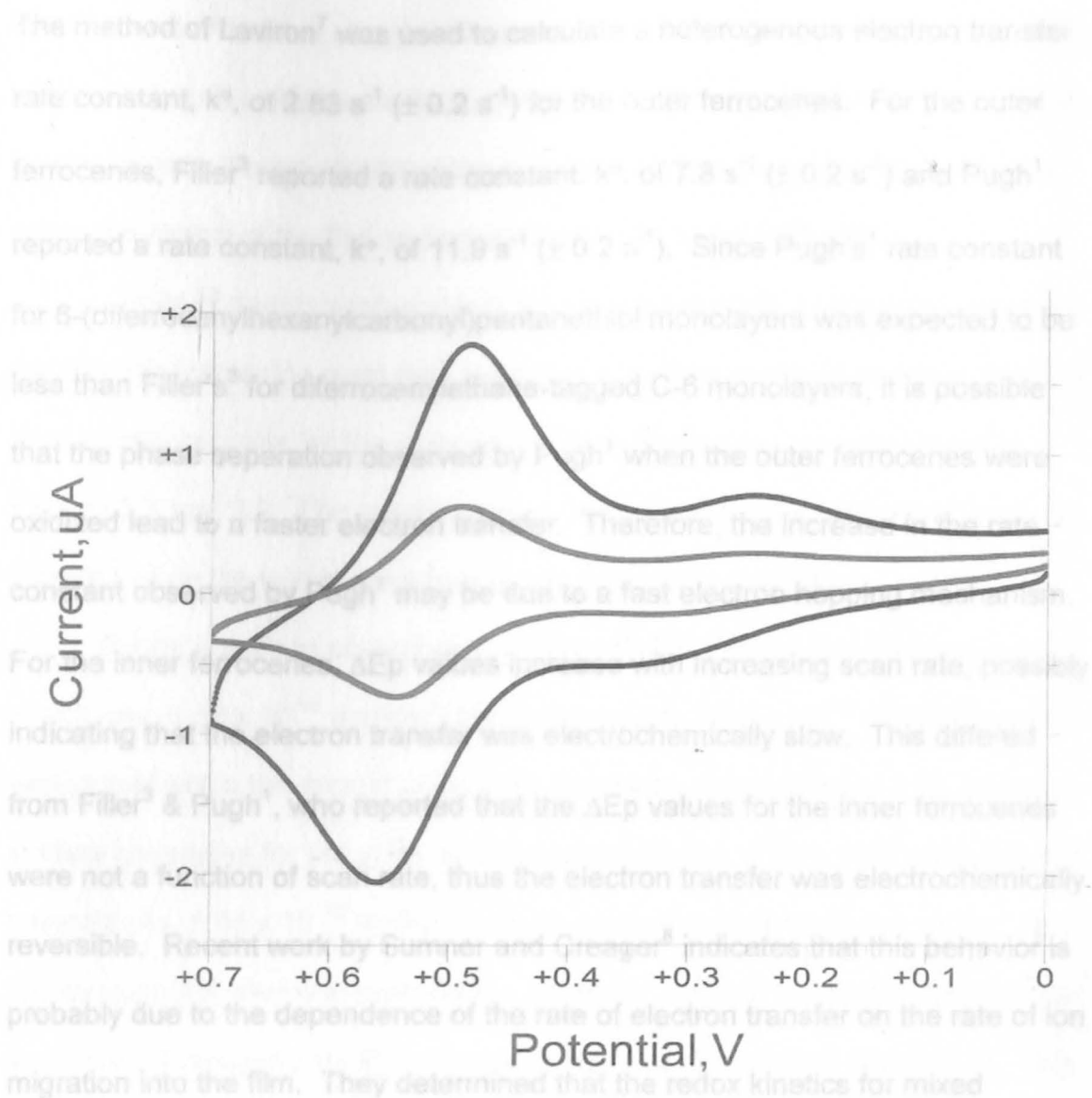


Figure 3.7: Cyclic voltammograms of a 6-(diferrocenyldodecanyl carbonyl)pentanethiol monolayer E11 illustrating the effect of increasing scan rate on wave broadening. Blue = 400 mV/sec, Red = 100 mV/sec.

The method of Laviron⁷ was used to calculate a heterogeneous electron transfer rate constant, k° , of 2.83 s^{-1} ($\pm 0.2 \text{ s}^{-1}$) for the outer ferrocenes. For the outer ferrocenes, Filler³ reported a rate constant, k° , of 7.8 s^{-1} ($\pm 0.2 \text{ s}^{-1}$) and Pugh¹ reported a rate constant, k° , of 11.9 s^{-1} ($\pm 0.2 \text{ s}^{-1}$). Since Pugh's¹ rate constant for 6-(diferrocenylohexanecarbonyl)pentanethiol monolayers was expected to be less than Filler's³ for diferrocenylethane-tagged C-6 monolayers, it is possible that the phase separation observed by Pugh¹ when the outer ferrocenes were oxidized lead to a faster electron transfer. Therefore, the increase in the rate constant observed by Pugh¹ may be due to a fast electron hopping mechanism. For the inner ferrocenes, ΔE_p values increase with increasing scan rate, possibly indicating that the electron transfer was electrochemically slow. This differed from Filler³ & Pugh¹, who reported that the ΔE_p values for the inner ferrocenes were not a function of scan rate, thus the electron transfer was electrochemically reversible. Recent work by Sumner and Creager⁸ indicates that this behavior is probably due to the dependence of the rate of electron transfer on the rate of ion migration into the film. They determined that the redox kinetics for mixed monolayers containing ferrocene terminated SAM's were much slower when the ferrocene groups were buried in the monolayer interior as compared to those ferrocene groups exposed to the electrolyte.⁸ Furthermore, the difference in electron transfer rate was found to be very dependent on the size of the charge compensating anion.⁸ Larger (polyanionic) anions, which are bulky, are more apt to slow down the electron transfer.⁸ Sumner and Creager⁸ reported that ready access to counter-ions is required for fast electron transfer to occur, and if

counter-ion transport is sluggish, then the overall rate could be set not by the rate of the electron transfer event itself, but rather by the rate of counter-ion transport. In other words, the rate-limiting step is most likely due to ion migration into the non-polar region of the film and not slow electron transfer kinetics.

Plots of anodic peak currents for each wave gives a slope that increases linearly with increasing scan rate, indicating a surface confined species. Plots of anodic peak currents for the inner ferrocenes versus scan rate are shown in Figures 3.8 and 3.9. The anodic peak currents for the outer ferrocenes were not included since the waves were very broad and poorly defined.

Average surface coverages (for E11 and E12) of the inner ferrocenes anodic (Av. 5.56×10^{-11} mol/cm²) and cathodic (Av. 5.90×10^{-11} mol/cm²) waves were equal within the margin of error for the measurement (Table 3.1). Average surface coverages for the outer ferrocenes anodic (Av. 4.84×10^{-12} mol/cm²) and cathodic (Av. 5.05×10^{-12} mol/cm²) waves were also essentially the same. This further supports chemical reversibility. However, surface coverages for the outer ferrocenes averaged only 8% of those for the inner ferrocenes (Table 3.1). This is considerably less than Pugh¹ observed, with the surface coverages for the outer ferrocenes (Av. 2.46×10^{-12} mol /cm²) being 40% of the inner ferrocenes (Av. 6.23×10^{-11} mol /cm²). Lewis⁴ confirmed that the surface coverages for the outer ferrocenes on the same 6-(diferrocenylhexanylcarbonyl)pentanethiol monolayers studied by Pugh¹ were 40-50% less than those observed for the inner ferrocenes. Filler³, on the other hand, reported similar surface coverages of 2×10^{-10} mol/cm² for both inner and outer ferrocenes in his study of

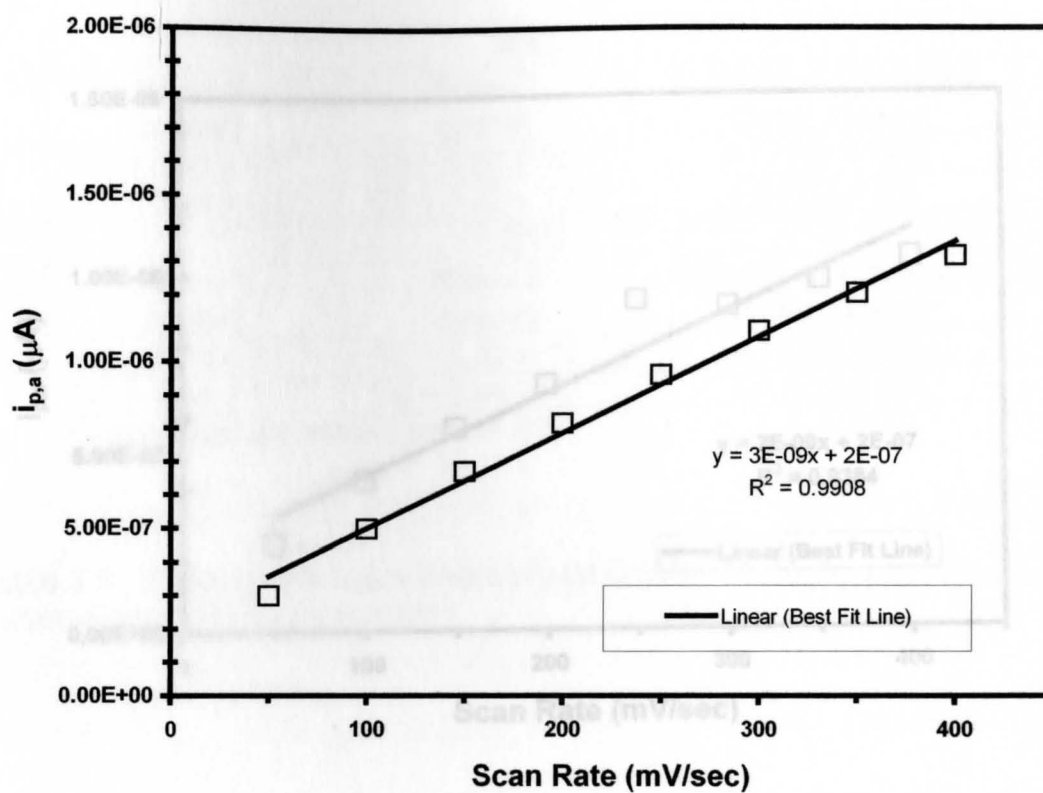


Figure 3.8: Anodic peak currents ($i_{p,a}$) for inner ferrocenes vs. scan rate for a 6-(diferrocenyldodecanylcarbonyl)pentanethiol monolayer on electrode E12

Figure 3.8: Anodic peak currents ($i_{p,a}$) for inner ferrocenes vs. scan rate for a 6-(diferrocenyldodecanylcarbonyl)pentanethiol monolayer on electrode E11

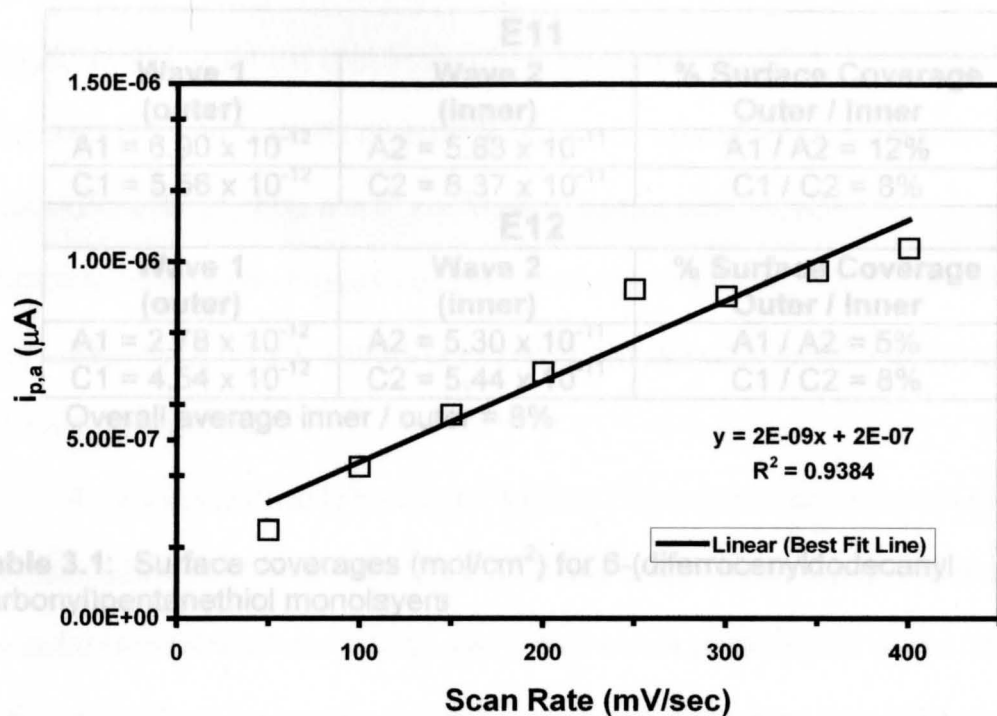


Figure 3.9: Anodic peak currents ($i_{p,a}$) for inner ferrocene vs. scan rate for a 6-(diferrocenyldodecanylcarbonyl)pentanethiol monolayer on electrode E12

E11		
Wave 1 (outer)	Wave 2 (inner)	% Surface Coverage Outer / Inner
A1 = 6.90×10^{-12}	A2 = 5.83×10^{-11}	A1 / A2 = 12%
C1 = 5.56×10^{-12}	C2 = 6.37×10^{-11}	C1 / C2 = 8%
E12		
Wave 1 (outer)	Wave 2 (inner)	% Surface Coverage Outer / Inner
A1 = 2.78×10^{-12}	A2 = 5.30×10^{-11}	A1 / A2 = 5%
C1 = 4.54×10^{-12}	C2 = 5.44×10^{-11}	C1 / C2 = 8%

Overall average inner / outer = 8%

Table 3.1: Surface coverages (mol/cm^2) for 6-(diferrocenyldodecanyl carbonyl)pentanethiol monolayers

A subsequent study by Lewis⁴ focused on conducting voltammetry in non-aqueous solvents. The study found that using such non-aqueous solvents did not increase the electrochemical accessibility for the outer ferrocenes in 6-(diferrocenyldodecanyl carbonyl)pentanethiol monolayers. It is possible that a more non-polar solvent, like methylene chloride, would show a different result.

The results observed here are also contrary to those observed in the literature by Campbell et al.⁹ who studied self-assembled monolayers with an inner azobenzene group and an outer ferrocene separated by alkane chains of

diferrocenylethane-tagged C-6 monolayers. The ferrocenes in Fillers³ monolayer were likely standing straight up (or at 27°) because of the shorter bridging alkane chain length. This would explain the greater electrochemical accessibility of the outer ferrocenes. Increased surface coverages were likely due to the smaller size of the head group. Pugh¹ suggested the observed electrochemical inaccessibility of the outer ferrocenes may be due to the majority of outer ferrocenes folding over into the non-polar region of the film.¹ This effect would be accentuated in 1,12-diferrocenyldodecane-tagged self-assembled monolayers, due to the longer intervening chain length, resulting in even lower electrochemical accessibility for the outer ferrocenes.

A subsequent study by Lewis⁴ focused on conducting voltammetry in non-aqueous solvents (0.1 M TBAP/THF) with the assumption that this might prevent the outer ferrocenes from folding over into the non-polar region of the monolayer. While the surface coverages for both ferrocenes decreased due to desorption in the non-aqueous solvent, the ratio of surface coverages remained the same. Therefore, Lewis⁴ study found that using such non-aqueous solvents did not increase the electrochemical accessibility for the outer ferrocenes in 6-(diferrocenylhexanylethyl)pentanethiol monolayers. It is possible that a more non-polar solvent, like methylene chloride, would show a different result.

The results observed here are also contrary to those observed in the literature by Campbell et al.⁹ who studied self-assembled monolayers with an inner azobenzene group and an outer ferrocene separated by alkane chains of

differing lengths. In these studies, the monolayers exhibited essentially total accessibility for the outer ferrocene groups but no accessibility for the inner azobenzenes group when the chain length between the two groups was four carbons long.⁹ One possible explanation for this difference may be that the reduction of azobenzene in the monolayer is a proton coupled electron transfer with hydrazobenzene formation.⁹ This is important because azobenzene oxidation / reduction involves both electron and proton transfer, the pH of the electrolyte has to be taken into consideration, as well as the effects of ion migration.⁸ Furthermore, azobenzene is a planar molecule, whereas ferrocene is treated as a sphere and packs much less densely. Therefore, it is possible that both the pH and the dense packing of the inner azobenzenes in Campbell et al's⁹ study are playing a role in the electrochemical inaccessibility of the inner groups. For the monolayers studied here, pH is less important since each of the ferrocenes undergoes a single, 1 electron transfer that is not coupled with a proton transfer.

Kubo¹⁰ and Horikoshi¹¹ synthesized and studied biferrocenyl terminated alkanethiols. In similarity to the behavior observed here, Kubo¹⁰ and Horikoshi¹¹ observed two, single electron transfers with oxidation of the outer ferrocene occurring at less anodic potentials versus the inner ferrocenes. This is due to the proximity of the inner ferrocenes to an electron withdrawing carbonyl group. However the biferrocenyl-tagged monolayers were chemically and electrochemically irreversible. In undiluted films the k° for the outer ferrocene, was $k_1 = 0.93 \text{ s}^{-1} (\pm 0.02 \text{ s}^{-1})$, and the k° for the inner ferrocene was $k_2 = 0.64 \text{ s}^{-1}$

($\pm 0.02 \text{ s}^{-1}$).¹⁰ The rate constant increased with decreasing surface coverage. Kubo¹⁰ postulated that the reason for the slower electron transfer kinetics of the SAM's with higher surface coverage could be electrostatic repulsion between charged biferrocenyl sites. It is possible that because of the proximity of the ferrocene groups, coulombic interactions may play a role, since counter-ions may interfere with the oxidation of the neighboring biferrocenyls.¹⁰

The FWHM values at a scan rate of 200 mV/sec for the first anodic and cathodic waves (outer ferrocenes) for both of the electrodes were not obtained since the peaks were very broad and poorly defined. The FWHM values for the second anodic and cathodic waves (inner ferrocenes) were well defined and determined by subtracting the potentials at half peak-height.¹ The FWHM values were essentially the same for the second anodic and cathodic waves at 125 mV and 121 mV, respectively. This indicates that there is some disorder in the monolayer since the value deviates from $90/n$ mV, that of a well organized monolayer.² In Chidsey's² study of mixed monolayers of ferrocene terminated and unsubstituted undecanethiol in 1M aqueous HClO_4 , the cyclic voltammograms broadened considerably as the mole fraction of the ferrocene containing thiol increased. In Chidsey's² work, when the mole fraction of ferrocene terminated thiol was 1, substantial broadening occurred, with FWHM values of approximately $300/n$ mV. Therefore, even though the differrocene-films examined here are not diluted with any non-electroactive thiol, they are still much more highly ordered than those observed by Chidsey.² This is likely due to the backside chain interactions that occur with the alkane chains that attach the inner

ferrocenes to the outer ferrocenes.¹² Such interactions have been shown to lead to more van der Waals interactions and thus explain the increase in order. The FWHM values determined by Pugh were 90 mV for the second wave, indicating order, but only 44.9 mV for the first anodic wave indicating a possible structural rearrangement or domain formation in the film.¹² Values of ~ 90 mV for an undiluted self-assembled monolayer are very unusual, as they are expected to show disorder. For the first anodic and cathodic waves, Filler³ reported FWHM values of 141 and 171 mV, respectively. For the second anodic and cathodic waves both values Filler³ reported 124 mV, which were similar to the values obtained here. The larger FWHM values are the result of disorder in the film. Thus, some of the ferrocenes are in different electrochemical environments, leading to a distribution of E° 's and broader peaks.

3.6 Conclusions

The four step synthesis of 6-(diferrocenyldodecanylcarbonyl)pentanethiol was completed, as detailed here. Intermediate and final products were characterized by mass spectrometry, ^1H and ^{13}C NMR and CV, as applicable. The solution voltammetry of the intermediate products, 1,12-diferrocenyl dodecane-1,12-dione and 1,12-diferrocenyldodecane was evaluated. The data indicated the diferrocene compounds were chemically and electrochemically reversible. In solution, both compounds exhibited a single, two-electron transfer that was under diffusion control. The E° 's were characteristic of carbonyl and alkyl substituted ferrocenes. The results from the solution voltammetry experiments were comparable to work completed by Pugh.¹

The electrochemical properties of 6-(diferrocenyldodecanylcarbonyl)pentanethiol monolayers adsorbed on gold electrodes was characterized and evaluated here. The voltammetric waves for the outer ferrocenes were broad and poorly defined. The inner ferrocene exhibited comparatively narrow waves that were fairly well defined. The monolayer voltammetry showed that oxidation of both ferrocenes was chemically reversible. The oxidation of the inner ferrocenes showed an increase in ΔE_p with increasing v . This is most likely due to slow ion migration and not slow electron transfer kinetics.⁸ The oxidation of the outer ferrocenes were found to be electrochemically irreversible, with a rate constant of $2.83 \text{ s}^{-1} (\pm 0.2 \text{ s}^{-1})$. The rate constant was less than those reported by Filler³ for diferrocenylethane-tagged C-6 monolayers (k° of $7.8 \text{ s}^{-1} (\pm 0.2 \text{ s}^{-1})$) and Pugh¹ for 6-(diferrocenylhexanylcarbonyl)pentanethiol monolayers (k° of $11.9 \text{ s}^{-1} (\pm 0.2 \text{ s}^{-1})$). Interestingly, Pugh's¹ rate constant is slightly larger than Filler's³, indicating the possibility of a structural rearrangement and a fast electron hopping mechanism.

The FWHM values for the inner ferrocenes were 125 and 121 mV for the inner anodic and cathodic waves, respectively. This is indicative of some disorder in the monolayer. This is comparable to the FWHM of the voltammetric waves observed by Filler³, but significantly more disordered than those reported by Pugh.¹ Of interest, Chidsey² in his study of mixed unsubstituted and electroactive ferrocene terminated thiols saw broad waves and FWHM values of $\sim 300/n$ mV for undiluted films. This indicated a large amount of disorder when no diluent alkanethiols were incorporated into the film.

The surface coverages of the outer ferrocenes were only 8% of those of the inner ferrocenes, meaning that most of the outer ferrocenes were electrochemically inaccessible. The limited accessibility of the outer ferrocenes in this study showed stark contrast to work completed by Campbell et al.⁹ in that in their work, the outer ferrocenes were totally accessible. Pugh¹, and subsequently Lewis⁴, saw similar results to those observed here, in that the outer ferrocenes only exhibited limited (40-50%) accessibility compared to that of the inner ferrocenes. Pugh¹ postulated that this could be due some of the outer ferrocenes folding over into the non-polar alkane region making them electrochemically inaccessible. A systematic study of non-polar solvents might be one way to empirically elucidate the plausibility of such an assertion.

In summary, the most unique aspect of the research here is the inaccessibility of the outer ferrocenes. As the alkane chain length that bridged the ferrocenes was increased from 2 to 6 to 12 carbons, the accessibility of the outer ferrocenes decreased markedly. In comparing the ratio of surface coverages of the inner / outer ferrocenes the following was determined; For 1,12-(diferrocenyldodecanylcarbonyl)pentanethiol monolayers only 8% of the outer ferrocenes were electrochemically accessible, for 6-(diferrocenyloctylcarbonyl)pentanethiol monolayers 40% of the outer ferrocenes were accessible, and for diferrocenyloctane-tagged C-6 monolayers essentially 100% of the outer ferrocenes were accessible.^{1,3} A comparison of effect of the alkane chain length bridging the ferrocenes on surface coverage is given in Figure 3.10.

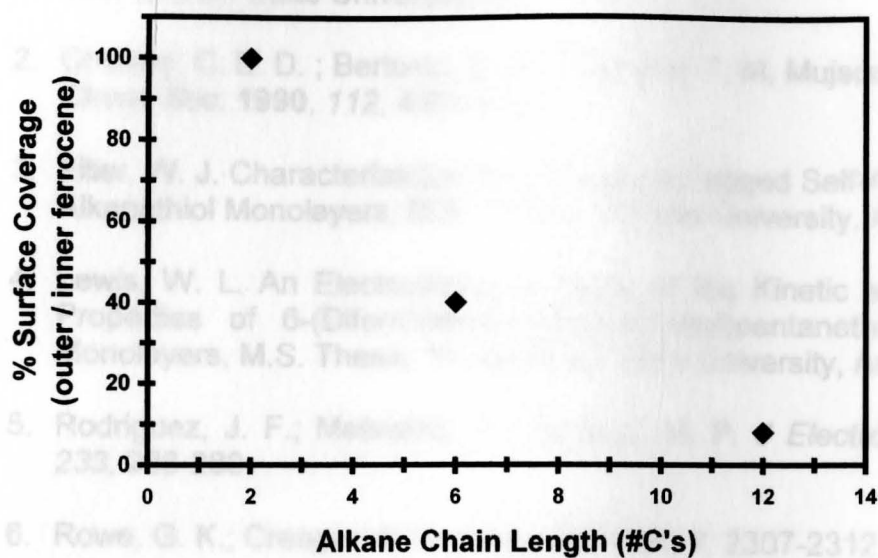


Figure 3.10: Effect of increasing bridging alkane chain length in diferrocene-tagged alkanethiol SAM's on electrochemical accessibility of the outer ferrocenes.^{1,3}

3.7 References

1. Pugh, C. A. Synthesis and Electrochemical Characterization of Novel Bridged Ferrocene Tagged Alkanethiol Self-Assembled Monolayers, M.S. Thesis, Youngstown State University, May 2001.
2. Chidsey, C. E. D. ; Bertozzi, C. R.; Putvinski, T. M, Majsce, A. M. *J. Am. Chem. Soc.* **1990**, *112*, 4301-4306.
3. Filler, W. J. Characterization of Diferrocene Tagged Self-Assembled Alkanethiol Monolayers, M.S. Thesis, Temple University, August, 1996.
4. Lewis, W. L. An Electrochemical Study of the Kinetic and Thermodynamic Properties of 6-(Diferrocenylohexanecarbonyl)pentanethiol Self-Assembled Monolayers, M.S. Thesis, Youngstown State University, August 2002.
5. Rodriguez, J. F.; Mebrahtu, T.; Soriaga, M. P. *J Electroanal. Chem.* **1987**, *233*, 283-289.
6. Rowe, G. K.; Creager, S. E. *Langmuir* **1991**, *7*, 2307-2312
7. Laviron, E. J. *Electroanal. Chem* **1979**, *101*, 19-28
8. Sumner, J. J.; Creager, S. E. *J. Phys. Chem. B* **2001**, *105*, 8739-8745.
9. Campbell, D. J.; Herr, B. R.; Hulteen, J. C.; Van Duyne, R. P, Mirkin, C. A. *J. Am. Chem. Soc.* **1996**, *118*, 10211-10219.
10. Kubo, K.; Kondow, H.; Nishihara, H. *Electrochemistry* **1999**, *12*, 1129-1131.
11. Horikoshi, T.; Itoh, M.; Kurihara, M; Kubo, K.; Nishihara, H. *J. of Electroanal. Chem.* **1999**, *1-2*, 113-116.
12. Ulman, A. *An Introduction to Ultrathin Organic Films*; Academic Press: New York, **1994**.